

# Supplementary Material for “Sources of marine debris for Seychelles and other remote islands in the western Indian Ocean”

Vogt-Vincent, N.S.<sup>1</sup>, Burt, A.J.<sup>2</sup>, Kaplan, D.<sup>3,4</sup>, Mitarai, S.<sup>5</sup>, Turnbull, L.A.<sup>2</sup>, Johnson, H.L.<sup>1</sup>

<sup>1</sup> *Department of Earth Sciences, University of Oxford, Oxford, United Kingdom*

<sup>2</sup> *Department of Plant Sciences, University of Oxford, Oxford, United Kingdom*

<sup>3</sup> *MARBEC, Univ Montpellier, CNRS, Ifremer, IRD, Sète, France*

<sup>4</sup> *Institut de Recherche pour le Développement (IRD), MARBEC, Sète, France*

<sup>5</sup> *Marine Biophysics Unit, Okinawa Institute of Science and Technology Graduate University, Okinawa, Japan*

## Supplementary Text 1: Particle tracking near the coast

There is a land-sea mask mismatch between ocean current output from GLORYS and Stokes drift output from WAVERYS, as they are computed on different grids. Simply summing these components would result in the Stokes drift component artificially dropping to zero in some regions. To bypass this issue, we adopted the regular interpolated 1/12° CMEMS GLORYS land-sea mask as the ‘true coast’, and used the `setmisstodis` operator in CDO (Schulzweida, 2021) to gap-fill Stokes drift in coastal regions (to avoid Stokes drift abruptly vanishing near the coast). We regridded ERA5 surface winds to the WAVERYS grid, and combined the resulting datasets to reduce the number of interpolations required by Parcels. For scenarios with more than set of forcings (i.e. CS0-5), these were added using an `OceanParcels SummedField` object.

We implemented beaching through postprocessing (see section 2.2), so it is important that particles do not explicitly ‘beach’ during particle tracking. Explicit beaching would occur frequently due to the nonzero winds (and Stokes drift, due to the above processing) over land. Although it would be possible to interpolate both the winds and Stokes drift to the higher resolution GLORYS land-sea mask and set velocities over land to zero, this would result in a prohibitively high storage requirement due to the higher time frequency of the wind and Stokes drift output. In addition, it would still be possible for particles to get stuck at the coast due to the use of a uniform diffusivity and the fact that particle velocities approach zero as they approach the coast when using linear interpolation on an A-grid (the CMEMS GLORYS data are provided on an interpolated A-grid). To avoid this, we used the `freeslip` interpolation method in OceanParcels, emulating free slip boundary conditions during particle tracking. A small fraction of particles still ‘beached’ due to stochastic diffusion and numerical error, so to entirely eliminate explicit beaching, we applied a velocity normal to the ‘coast’ once they approached within 0.5 grid cells of the coastline, with the strength ramping up with proximity to the coast.

## Supplementary Text 2: Offline calculation of beached debris

Following the assumptions stated in section 2.2, the rate of change of mass  $M_i$  represented by a particular particle  $j$  influenced by a constant sinking rate  $\mu_s$  and a beaching rate  $\mu_b$  is given by

$$\begin{aligned}\frac{dM_j}{dt} &= -(\mu_s + \mu_b(t))M_j \\ M_j(0) &= M_j^0\end{aligned}$$

where the beaching rate  $\mu_b(t) = \mu_b^*$  when a particle is within a coastal grid cell, and 0 otherwise. The solution to this differential equation is

$$\begin{aligned}M_j(t) &= M_j^0 \cdot \exp(-\mu_s t - \phi(t)) \\ \phi(t) &= \int_0^t \mu_b(\tau) d\tau\end{aligned}$$

If we define a ‘beaching event’ as the time spent by a particle in a coastal cell, then the mass  $m_{jk}$  beached by particle  $j$  during beaching event  $k$ ,  $t_k^0 \leq t \leq t_k^0 + \Delta t_k$ , is given by

$$\begin{aligned}m_{jk} &= \int_{t_k^0}^{t_k^0 + \Delta t_k} \mu_b^* M_j(\tau) d\tau \\ &= \mu_b^* M_j^0 \int_{t_k^0}^{t_k^0 + \Delta t_k} \exp(-\mu_s \tau - \phi(\tau)) d\tau\end{aligned}$$

(1)

It would be possible to calculate  $m_{jk}$  offline by saving the position  $(x, y, t)$  of each particle at regular time intervals, approximating  $\phi(t)$  by evaluating the coastal status at each particle position, and solving equation (1) numerically. However, there are over  $2 \times 10^{11}$  particles across all our simulations and capturing every beaching event would require a sampling period of  $\frac{\sim 8000 \text{ m}}{\sim 1 \text{ ms}^{-1}} \approx 2\text{h}$ , or around 44,000 samples over a 10 year integration. By storing  $(x, y)$  as 16-bit cell indices and assuming a constant time step between samples, one complete trajectory could be stored in 176kB (uncompressed). For all particles, this would result in a storage requirement of over 30PB. Even allowing for compression and permitting a coarser sampling frequency, this would still result in an unmanageable storage requirement.

Alternatively, equation (1) could be solved online (i.e. during particle tracking), greatly reducing storage requirements, as only  $m_{jk}$  and the associated beaching site would have to be stored (for instance, as a 16-bit float and 8-bit integer respectively) for each beaching event. Assuming an average of  $\sim 10$  beaching events per particle, this would reduce the raw storage requirement by almost 4 orders of magnitude to around 6TB (and likely lower with compression). Unfortunately, solving this equation online means that  $\mu_s$  and  $\mu_b$  must be defined at run-time, so particle tracking would have to be rerun for every  $(\mu_s, \mu_b^*)$  configuration of interest. Given the computational cost involved in simulating the trajectories of order  $10^{11}$  particles, this is undesirable.

However, there is a piecewise analytical solution to equation (1). Within a particular beaching event  $k$ ,  $t_k^0 \leq t \leq t_k^0 + \Delta t_k$ :

$$\begin{aligned}\phi_k^0(t) &= \int_0^t \mu_b(\tau) d\tau \\ &= \phi_k^0 + \mu_b^*(t - t_k^0)\end{aligned}$$

where  $\phi_k$  is  $\phi$  during beaching event  $k$ , and  $\phi_k^0 = \phi(t_k^0)$ . Therefore:

$$\begin{aligned}m_{jk} &= \mu_b^* M_j^0 \int_{t_k^0}^{t_k^0 + \Delta t_k} \exp(-\mu_s \tau - \phi_k^0 - \mu_b^*(\tau - t_k^0)) d\tau \\ &= -\frac{\mu_b^* M_j^0}{\mu_s + \mu_b^*} \left[ \exp(-\mu_s \tau - \phi_k^0 - \mu_b^*(\tau - t_k^0)) \right]_{t_k^0}^{t_k^0 + \Delta t_k} \\ &= \frac{\mu_b^*}{\mu_s + \mu_b^*} (M_j(t_k^0) - M_j(t_k^0 + \Delta t_k))\end{aligned}\tag{2}$$

Equation (2) shows that, as long as we store the variables  $t_k^0$ ,  $\Delta t_k$ ,  $\phi_k^0$ , and the sink cell index  $j$  for every beaching event  $k$ , we can perfectly reconstruct all  $m_{jk}$ . In our model configuration, these four variables can be stored as one 64-bit integer. By using this method, it is possible to recompute  $m_{jk}$  for different beaching and sinking rates (at very low computational cost relative to rerunning the particle tracking), whilst also minimising storage requirements. We have run these simulations using an OceanParcels kernel that tracks these four variables and saves them at the end of every beaching event. Compressed, our simulations have a total storage requirement of c. 1 TB, which is very manageable on inexpensive modern hardware.

### Supplementary Text 3: Backward experiments to constrain potential sources

We carried out computationally inexpensive backtracking experiments to identify which countries could potentially act as sources of debris for Seychelles. We released approximately  $5.1 \times 10^7$  particles from islands across Seychelles (spread across monthly releases), and backtracked them for up to 27 years following surface currents and Stokes drift (no windage), regularly outputting each particle position  $\mathbf{x}$ , age  $t$ , and the time spent in coastal grid cells  $t_b$ , i.e. an observation  $i$  is given by the set  $(\mathbf{x}, t, t_b)$ . From these data, for every particle position, we then calculated the proportion of mass  $f_M^i(t, t_b)$  that would remain once the particle reached Seychelles, using the following equation:

$$f_M^i(t, t_b) = \exp(-\mu_s t - \mu_b t_b)$$

For  $\mu_s = 1/30y$ , and  $\mu_b = 1/20d$  as a pessimistic estimate. We then gridded all  $f_M^i(t, t_b)$  to a regular grid, resulting in a list of  $f_M(t, t_b)$  associated with each grid cell. To obtain a reasonable worst-case estimate, we then took the 90<sup>th</sup> percentile (highest)  $f_M(t, t_b)$  for each grid cell. The result is Supplementary Figure 1. In short, the colour of each grid cell in SF1 gives the (90<sup>th</sup> percentile of the) proportion of debris passing through that cell that reaches Seychelles. However, it is important to remember that since this preliminary analysis is based on a backtracking experiment, all trajectories necessarily end at Seychelles. SF1 is therefore an absolute worst-case estimate. For instance, SF1 shows that particles leaving the coast of Angola in southwestern Africa only lost a small proportion of their mass through beaching and sinking before arriving at Seychelles. However, the full forward experiments demonstrate that only an extremely small proportion of trajectories originating from Angola reached Seychelles, so Angola is not a significant source of debris for Seychelles.

Winds were not included in this preliminary experiment. Based on climatological wind patterns, this preliminary experiment may underestimate the likelihood of debris reaching Seychelles from the western coast of the Americas and Brazil. However, the enormous size of the Pacific and relatively small sources of debris along the western coast of the Americas makes this an unlikely source of debris for most of the WIO, and based on our full forward model, *if* Brazil is a significant source for any WIO islands, it likely only affects Réunion and Mauritius.

### List of source sites identified as potential sources of debris for Seychelles and included in the full forward model

Angola, Argentina, Australia, Bahrain, Bangladesh, Brazil, Brunei Darussalam, Cambodia, Chagos Archipelago, China, Christmas Island, Cocos (Keeling) Islands, Comoros, Djibouti, Egypt, Eritrea, Falkland Islands, Hong Kong, India, Indonesia, Iran, Iraq, Japan, Jordan, Kenya, Kuwait, Macao, Madagascar, Malaysia, Maldives, Mauritius, Mayotte, Mozambique, Myanmar, Namibia, New Caledonia, New Zealand, Oman, Pakistan, Papua New Guinea, Philippines, Qatar, Réunion, Saudi Arabia, Seychelles, Singapore, Solomon Islands, Somalia, South Africa, Sri Lanka, Sudan, Taiwan, Tanzania, Thailand, Timor-Leste, United Arab Emirates, Uruguay, Vanuatu, Viet Nam, Yemen

### Supplementary Text 4: Constraints on $\mu_b^*$ from the Global Drifter Program and drifting Fish Aggregating Devices

Based on a dataset of (1) drifters from the Global Drifter Program (GDP) and (2) dFADs, we estimated the model parameter  $\mu_b^*$ , i.e. the probability per unit time that debris beaches, given that it is within  $1/12^\circ$  of the coast. To do this, we evaluated whether a drifter was within  $1/12^\circ$  of the coast every time it reported its position, and then calculated the total time spent within  $1/12^\circ$  of the coast by the time it beached.

Evaluating whether a drifter has beached is not straightforward. For GDP drifters, we assessed this through four methods:

1. A GDP drifter has beached if its last reported position is less than 500m from the coastline (using the GSHHG shorelines database, Wessel & Smith, (1996))
2. A GDP drifter has beached if its last reported position is in less than 30m water depth (the typical length of a GDP drogue), based on the GEBCO2021 dataset.
3. A GDP drifter has beached if its death code assesses that it had a >90% chance of being beached (Lumpkin et al., 2012).
4. A GDP drifter has beached if the elevation 1km to the N/E/S/W of the last reported drifter location has an elevation of >0m (the criterion used in Kaandorp et al., (2020)).

We can extract the parameter  $\mu_b^*$  by (1) calculating the proportion of drifters still afloat that beach per day spent within  $1/12^\circ$  of the coast, or (2) finding a least-squares best fit of a curve in the form  $\exp(-\mu_b t)$  to the proportion of drifters still afloat after spending time  $t$  within  $1/12^\circ$  of the coast. The results are shown in Supplementary Figure 3. The proximity criterion appears to be the most conservative method, returning  $\mu_b^* \approx 1/45\text{d}$ . The GDP death code criteria was the least conservative, returning  $\mu_b^* \approx 1/10\text{d}$ . All methods returned a roughly uniform  $\mu_b^*$ , apart from the GDP death code criterion.

We assessed whether dFADs had beached using the following four methods:

1. A dFAD has beached if its last reported position is less than 500m from the coastline (using the GSHHG shorelines database, Wessel & Smith, (1996))
2. A dFAD has beached if its last reported position is in less than 30m water depth (the typical length of a GDP drogue), based on the GEBCO2021 dataset.
3. A dFAD has beached if its death code assesses that it had a >90% chance of being beached (Lumpkin et al., 2012).
4. A dFAD has beached based on beaching events detected through a stagnation threshold in Imzilen et al. (2021)

Many dFADs beached and subsequently unbeached according to the analysis by Imzilen et al. (2021) so, as we are primarily concerned with ‘terminal’ beaching events in this study, we only considered ‘final’ beachings as true beachings for the evaluation of  $\mu_b^*$ . All of the above methods produced time-varying estimates of  $\mu_b^*$  apart from the criterion used by Imzilen et al. (2021), which was approximately constant for  $t > 3d$ . The estimate for  $\mu_b^*$  based on the Imzilen et al. (2021) criterion was returning  $\mu_b^* \approx 1/20d$ .

On the basis of these analyses, we suggest that  $1/45d < \mu_b^* < 1/20d$ . Drifters and dFADs have long drogues which may get tangled in shallow water, potentially resulting in them being more likely to beach than undrogued debris. However, we note that Kaandorp et al., (2020) obtained an estimate of  $\mu_b^* = 1/24d$ , based on their  $1/16^\circ$  resolution grid. Scaling this up to our  $1/12^\circ$  resolution grid, this results in an expected value of  $\mu_b^* = 1/32d$ . This is within the range of reasonable values inferred from our analysis of GDP and dFAD beaching rates, so we have used a value of  $\mu_b^* = 1/30d$  in this study. However, we note that our estimates of source distribution are generally relatively insensitive to the value of  $\mu_b^*$  (see Supplementary Figures 20-22).

## Supplementary Text 5: Robustness of time-integral terrestrial source analyses

To test whether the time-integral predictions in main text Figure 4 are robust with respect to rare beaching ‘pulses’, we split plastic release years into two halves (1993-2003 and 2004-2014) and recalculated the source distributions using only the first or second half of release years. The resulting sets of source distributions are generally very similar, particularly in the case of the larger islands and island groups, which are naturally less sensitive to small-scale debris pulses. However, there are some localised differences.

The proportion of Class C debris beaching at the Seychelles Plateau attributable to Indonesia decreases when only considering the last half of release years (although still remains the largest single country of origin, with the exception of the northernmost island considered, Bird Island). The proportion of Class B debris reaching the Aldabra Group attributable to Indonesia decreases when only considering the last half of release years, although again remains the largest single source country for the Aldabra Group (with the exception of Cosmoledo). For Class A debris, marine debris beaching at the Aldabra and Farquhar Groups is dominated by two large pulses in 1995 and 1998 (main text Figure 5(a)) and, when considering the last half of release years only, the single largest source of Class A debris becomes Madagascar.

As a result, whilst our simulation timespan (with 22 debris release years for terrestrial debris) appears to have been sufficient for most sink sites and debris classes, this may not be true for Class A debris at all sites, as the primary source changed for two island groups when subsetting the time-series (although in neither case is Class A debris expected to account for a large proportion of beaching

debris). Some marine debris attribution studies which report results for remote islands have used considerably fewer release year (Chassignet et al., 2021; van der Mheen et al., 2020), which does raise questions as to how robust certain conclusions may be, although neither study considered short-lived plastics.

## Supplementary Text 6: Estimates of mean terrestrial beaching rates on Aldabra

Our analyses provide an estimate of the mean annual (terrestrial) debris beaching rates  $\bar{B}$  at various sites assuming a constant rate of debris input into the oceans (based on emissions in 2015, (Lebreton & Andrady, 2019; Meijer et al., 2021)), by averaging the accumulation rate from 1995-2014 (allowing for a 2-year 'spin-up'). However, the mass of debris entering the ocean has increased significantly through time (Geyer et al., 2017). Here, we outline three suggestions to convert the total mass  $M_{\text{Ald}}$  of terrestrial debris on Aldabra (approximately 87.3 tonnes (Burt et al., 2020)) into an average beaching rate based on 2015 emissions  $\bar{B}$ , which can be directly compared to our analyses.

### Method 1: Assume the rate of debris beaching is proportional to the rate at which plastic is discarded

Geyer et al. (2017) estimate the mass of plastic waste  $D_i$  discarded per year  $i$  from 1950 to 2015. By assuming that the fraction of discarded waste that enters the ocean remains constant, the ratio  $R_{\text{Geyer}}$  of the total mass of waste that has entered the ocean to the mass of waste entering the ocean in 2015 is:

$$R_{\text{Geyer}} = \frac{\sum_{i=1950}^{2015} D_i}{D_{2015}} = 30.5$$

Therefore:

$$\bar{B}_{\text{Geyer}} = \frac{M_{\text{Aldabra}}}{R_{\text{Geyer}}} = 2.9 \text{ tonnes y}^{-1}$$

### Method 2: Assume the rate of debris beaching at Aldabra is proportional to the number of items observed beaching per year at Cousine Island, Seychelles

Dunlop et al. (2020) summarise the results of almost two decades of marine debris monitoring at Cousine Island, Seychelles, providing estimates of accumulation rates (in terms of items per metre per day). for 10 years between 2003 and 2019. If we assume that interannual variability in marine debris accumulation at Cousine Island (not explicitly included as a sink in this study, but closest to Praslin) mirrors that at Aldabra, we can estimate  $R_{\text{Dunlop}}$  based on the observations in Dunlop et al. (2020). If we define  $A_i$  as the accumulation rate for year  $i$  at Cousine Island, where  $A_i$  is set to the observed annual accumulation rate for years with data, and linearly interpolated between the nearest years otherwise, then we can compute  $R_{\text{Dunlop}}$  as:

$$R_{\text{Dunlop}}^{\text{low}} = \frac{\sum_{i=2003}^{2015} A_i}{A_{2015}} = 16.5$$

$$R_{\text{Dunlop}}^{\text{high}} = \frac{\sum_{i=1950}^{2015} A_i}{A_{2015}} = 20.3$$

Where we assume  $A_{i < 2003} = 0$  for  $R_{\text{Dunlop}}^{\text{low}}$ , and  $A_{1950} = 0$  (based on Geyer et al. (2017)) for  $R_{\text{Dunlop}}^{\text{high}}$  (treating  $A_{1950} = 0$  as another datapoint and linearly interpolating between 1950 and the first actual observation in 2003). Therefore:

$$\bar{B}_{\text{Dunlop}}^{\text{low}} = \frac{M_{\text{Aldabra}}}{R_{\text{Dunlop}}^{\text{low}}} = 5.3 \text{ tonnes y}^{-1}$$

$$\bar{B}_{\text{Dunlop}}^{\text{high}} = \frac{M_{\text{Aldabra}}}{R_{\text{Dunlop}}^{\text{high}}} = 4.3 \text{ tonnes y}^{-1}$$

As a result, our first-order estimates suggest that the annual beaching rate of terrestrial debris at Aldabra should be around 2.9-5.3 tonnes per year, possibly on the lower end as our results in Section 3.2 suggest that interannual variability is considerably different between Aldabra and Praslin (and by extension, nearby Cousine).

### Supplementary Animation 1: Particle tracking near the coast

The efficient source-to-beaching method used in this study (as described in the main text and Supplementary Text 2) makes it more difficult to intuitively visualise transportation pathways, as we do not explicitly store particle positions. To aid interpretation, we ran another simulation, with debris represented as Class C debris (i.e.  $1/\mu_b^* = 30$  days,  $1/\mu_s = 360$  days, physical scenario CS3), but saving the particle state  $(x, y, t, M)$  every 24 hours, where the debris mass represented by the particle  $M$  is now computed *online* (in contrast with our main analyses), by integrating the following differential equation from Supplementary Text 2 using Forward Euler, with a time-step of 1 hour:

$$\frac{dM}{dt} = -(\mu_s + \mu_b(t))M$$

Using the same number of particles as in the main analyses would require an unreasonable amount of storage. Since this simulation was used for visualisation purposes only, we considered it reasonable to use a significantly smaller number of particles, namely 89,538 per release, by using a higher minimum debris flux threshold (5 tons per cell), and seeding parameters  $(c_1, c_2) = (2, 3.4)$ . We carried out releases two times per month, (half as frequently as the main analysis), from January 2015 to December 2018, for a total of 96 releases and approximately  $8.6 \times 10^6$  particles.

From these simulations, we then gridded all  $(x, y, t, M)$  records to a set of 2D histograms (one for each time index), with a regular bin spacing of  $0.05^\circ$ . We then passed each 2D histogram through a 2D Gaussian filter, with standard deviation  $0.1^\circ$ . This conserves the total mass of debris represented in each histogram, but compensates somewhat for the smaller particle count by improving the visibility of regions of sparse particle density. We finally computed the debris (mass) concentration by dividing the debris mass per bin by the surface area of each cell, and generated an animation from the result (Supplementary Animation 1).

## Supplementary Tables

Class A terrestrial debris		
Beaching site	Seasonal cycle peak	Seasonality strength
Aldabra	February	2170
Assomption	February	2110
Cosmoledo	February	1600
Astove	February	589
Providence	January	83.8
Farquhar	January	96.8
Alphonse	February	140
Poivre	February	52.4
St Joseph	February	43.9
Desroches	February	50.1
Platte	February	79.7
<i>Coëtivy</i>	<i>November</i>	<i>10.1</i>
Mahé	March	1.6
Fregate	February	53.6
Silhouette	June	2.4
Praslin	January	4.1
Denis	February	5.7
Bird	March	7.1
Comoros	December	1.6
Mayotte	December	7.2
Lakshadweep	January	173
Maldives	January	49.2
Mauritius	January	2.1
Réunion	January	1.5
Pemba	January	4.3
Socotra	January	4.1
Chagos Archipelago	November	36.2

**Table 1:** Class A debris beaching rate seasonal peak, and strength of the seasonal cycle (1995-2014), based on the phase of the component of the Fourier spectrum with period 1 year. The strength of the seasonal cycle is the ratio of the mean beaching rate during the three months with the highest beaching rate, and the three months with the lowest beaching rate. All time series correlated significantly with idealised cycle ( $p < 0.01$ ) aside from sites in italics.

Class B terrestrial debris		
Beaching site	Seasonal cycle peak	Seasonality strength
Aldabra	March	92.3
Assomption	March	162
Cosmoledo	March	91.7
Astove	March	594



Providence	March	21.7
Farquhar	March	107
<i>Alphonse</i>	<i>January</i>	<i>7.1</i>
<i>Poivre</i>	<i>November</i>	<i>4.6</i>
<i>St Joseph</i>	<i>December</i>	<i>5.0</i>
<i>Desroches</i>	<i>November</i>	<i>4.9</i>
<i>Platte</i>	<i>December</i>	<i>4.8</i>
<i>Coëtivy</i>	<i>January</i>	<i>7.1</i>
<hr/>		
Mahé	January	2.1
Fregate	January	7.9
<i>Silhouette</i>	<i>June</i>	<i>1.9</i>
Praslin	January	5.4
<i>Denis</i>	<i>February</i>	<i>5.5</i>
Bird	February	7.2
<hr/>		
Comoros	December	1.8
Mayotte	January	7.4
Lakshadweep	February	268
Maldives	February	24.6
Mauritius	January	2.4
Réunion	January	1.9
Pemba	January	5.3
Socotra	February	8.5
Chagos Archipelago	October	16.1

**Table 2:** Class B debris beaching rate seasonal peak, and strength of the seasonal cycle (1995-2014), based on the phase of the component of the Fourier spectrum with period 1 year. The strength of the seasonal cycle is the ratio of the mean beaching rate during the three months with the highest beaching rate, and the three months with the lowest beaching rate. All time series correlated significantly with idealised cycle ( $p < 0.01$ ) aside from sites in italics.

## Supplementary Figures

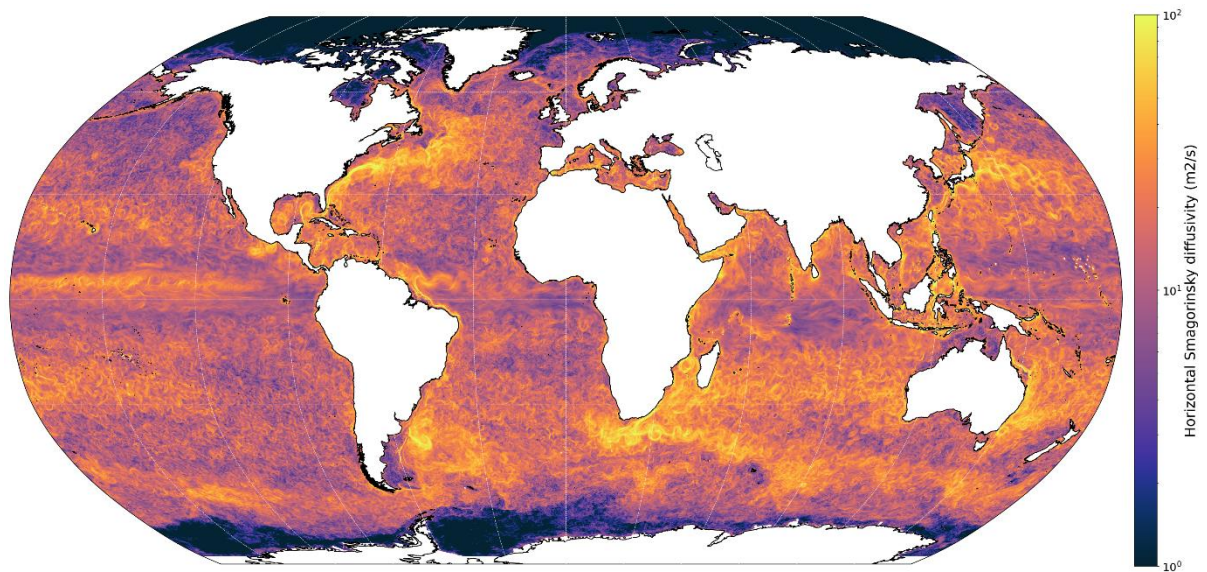


**Figure 1:** Horizontal Smagorinsky diffusivity diagnosed from daily surface velocity from GLORYS12V1, across one month (December 2019).

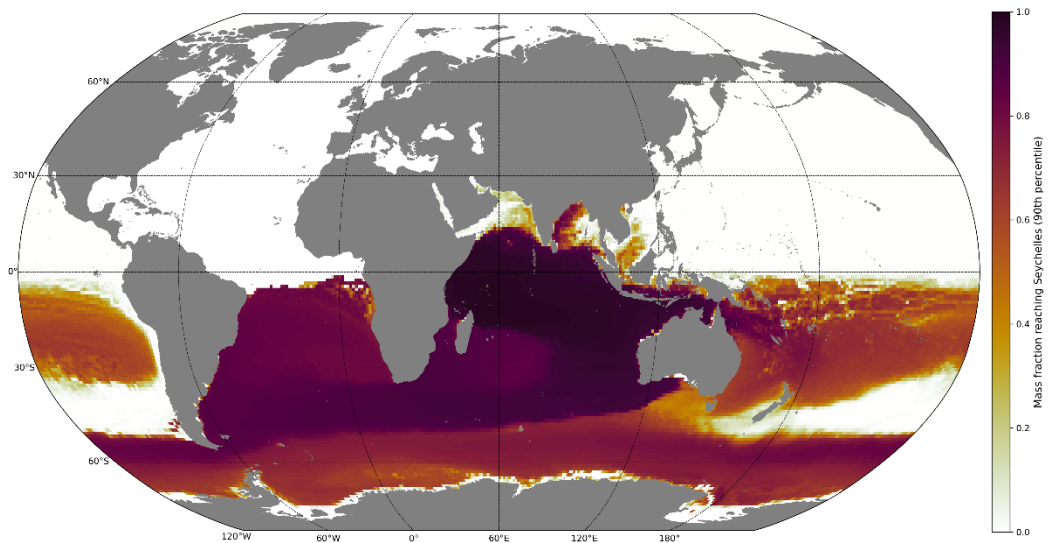


**Figure 2:** Mass fraction of debris from each grid cell remaining available for beaching upon arrival at Seychelles, based on backtracking experiments from Seychelles ( $\mu_b^* = 20d$ ,  $\mu_s = 30y$ , scenario CS0). This experiment does not take into account sources of marine debris so high values do not necessarily indicate that a significant quantity of debris arrives at Seychelles from a location, it simply means that of the trajectories that reached Seychelles from that location, losses from beaching and sinking from minor. In other words, cells appearing as white are very unlikely to be sources of debris for Seychelles, but coloured cells are not necessarily sources of debris for Seychelles. This, combined with a very conservative value for  $\mu_s$ , provides us with a list of most countries that could feasibly be sources of debris for Seychelles.

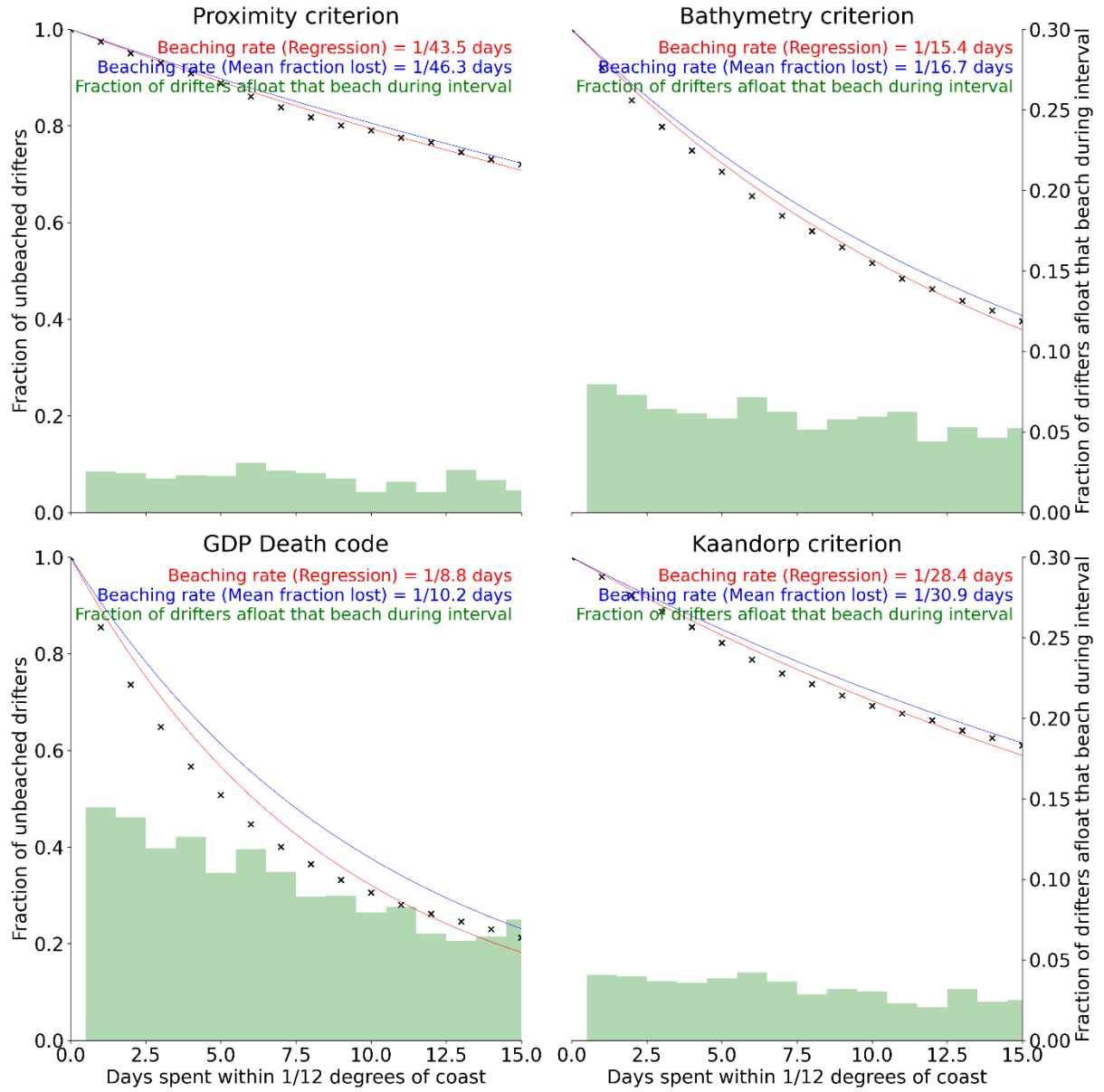


**Figure 3:** Estimates of  $\mu_b^*$  inferred from observations of drifters from the Global Drifter Program (Lumpkin & Centurioni, 2019) based on four different methodologies to assess whether a drifter has beached: (i) a trajectory terminating within 500m of the coast based on GSHHG, (ii) a trajectory terminating in less than 30m water depth based on GEBCO2021, (iii) a death code of 'beached' GDP drifter using a 90% likelihood threshold (Lumpkin et al., 2012), (iv) the beaching criterion used in Kaandorp et al. (2020), i.e. based on whether at least one point 1km to the N/E/S/W has an elevation >0m.

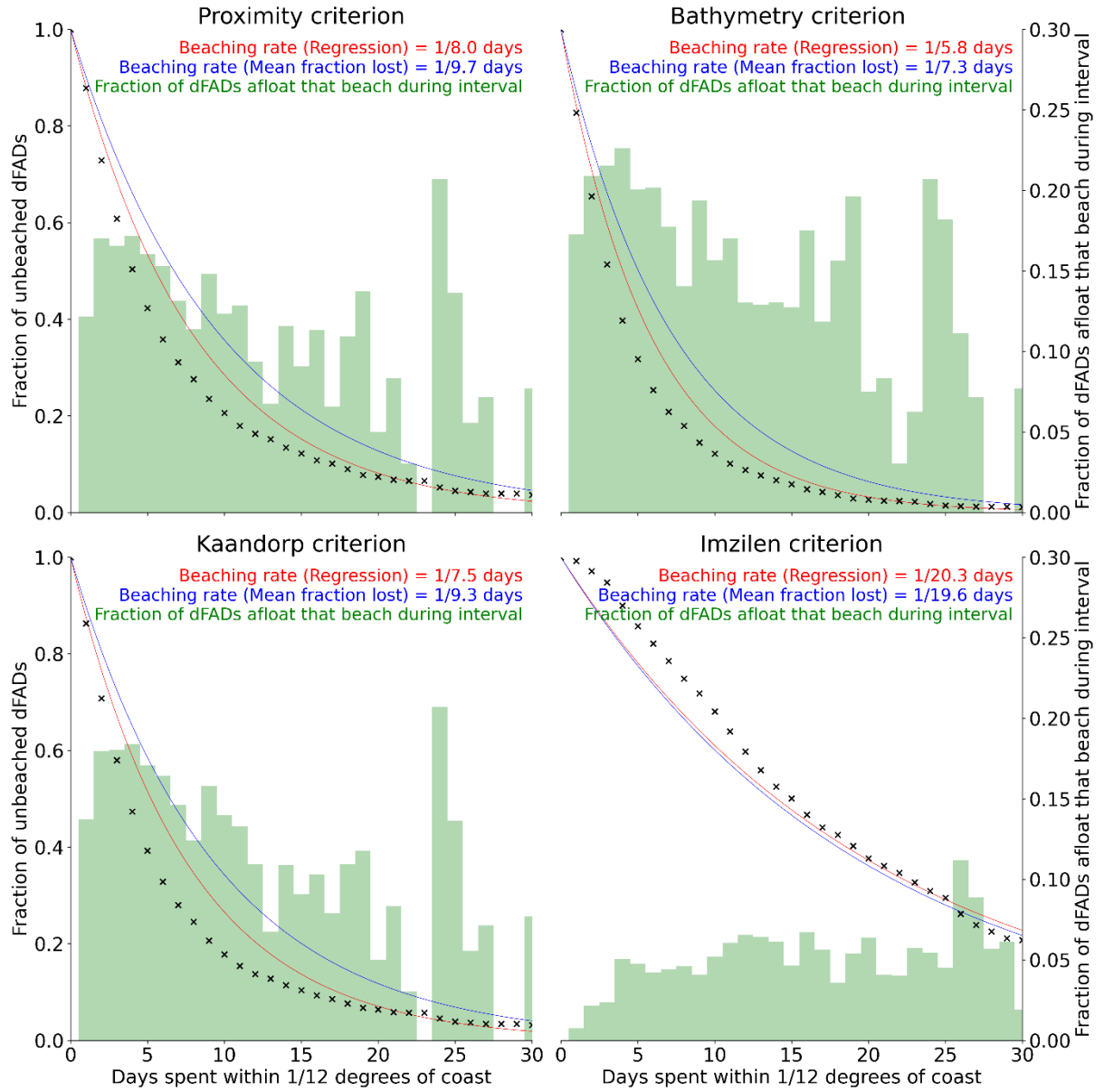


**Figure 4:** Estimates of  $\mu_b^*$  inferred from observations of dFADs in the Indian Ocean based on four different methodologies to assess whether a drifter has beached: (i) a trajectory terminating within 500m of the coast based on GSHHG, (ii) a trajectory terminating in less than 30m water depth based on GEBCO2021, (iii) the beaching criterion used in Kaandorp et al. (2020), i.e. based on whether at least one point 1km to the N/E/S/W has an elevation >0m, and (iv) beaching events identified by Imzilen et al. (2021).

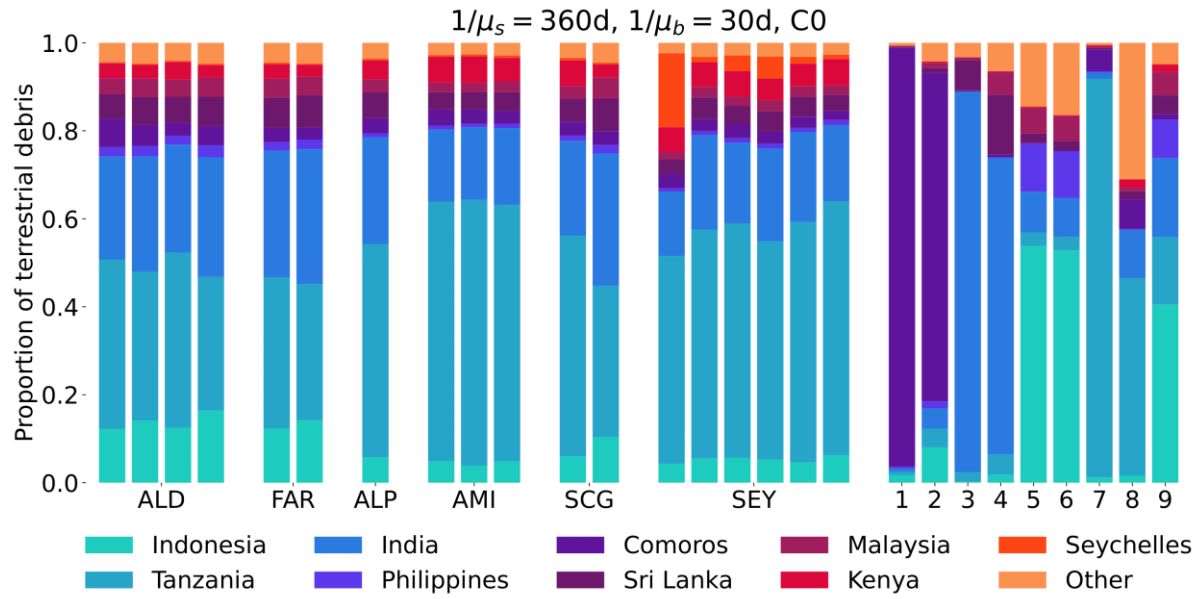


**Figure 5:** Equivalent to Figure 4 in the main text but for fixed sinking and beaching rate ( $1/\mu_s = 360d, 1/\mu_b = 30d$ ) and physical scenario C0 (i.e. surface currents only)

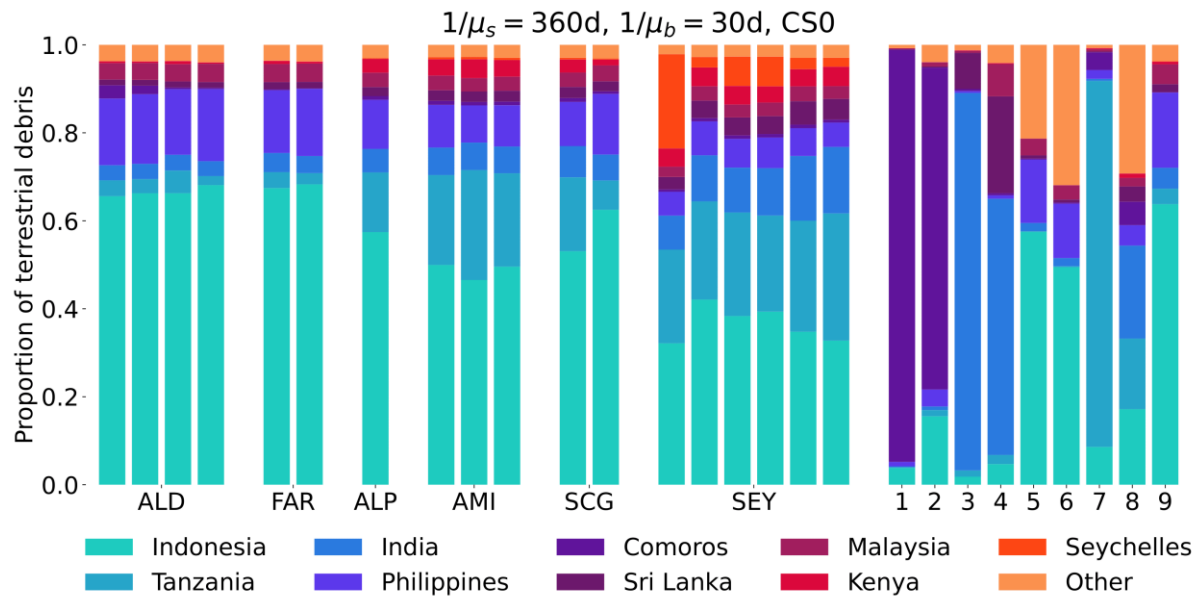


**Figure 6:** Equivalent to Figure 4 in the main text but for fixed sinking and beaching rate ( $1/\mu_s = 360d, 1/\mu_b = 30d$ ) and physical scenario CS0 (i.e. surface currents and Stokes drift)

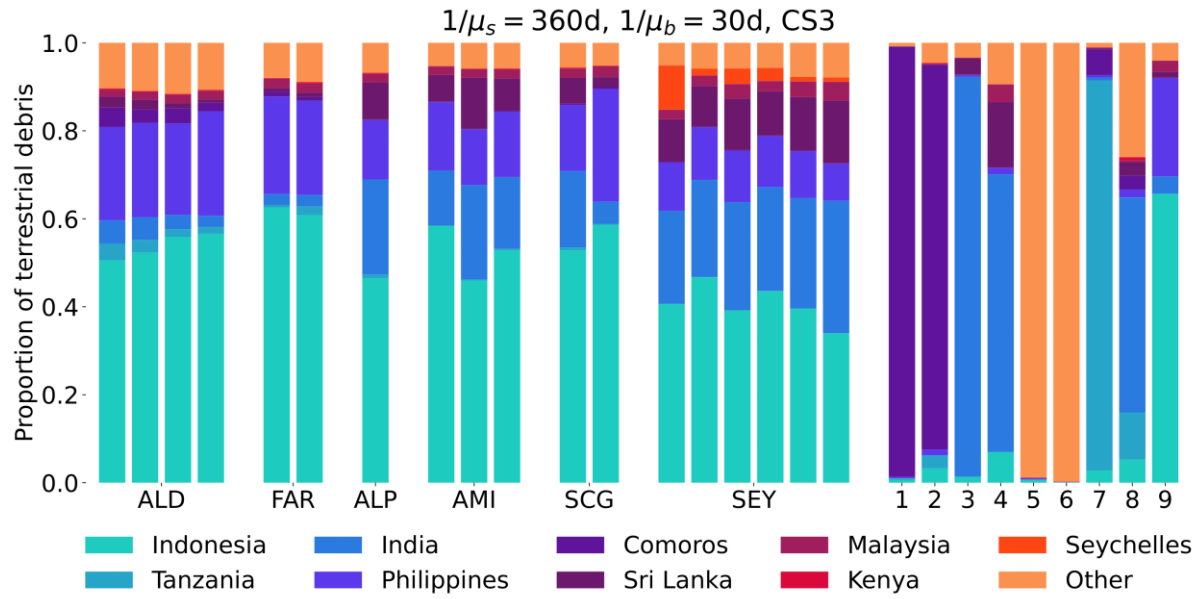


**Figure 7:** Equivalent to Figure 4 in the main text but for fixed sinking and beaching rate ( $1/\mu_s = 360d, 1/\mu_b = 30d$ ) and physical scenario CS3 (i.e. surface currents and Stokes drift and 3% windage)

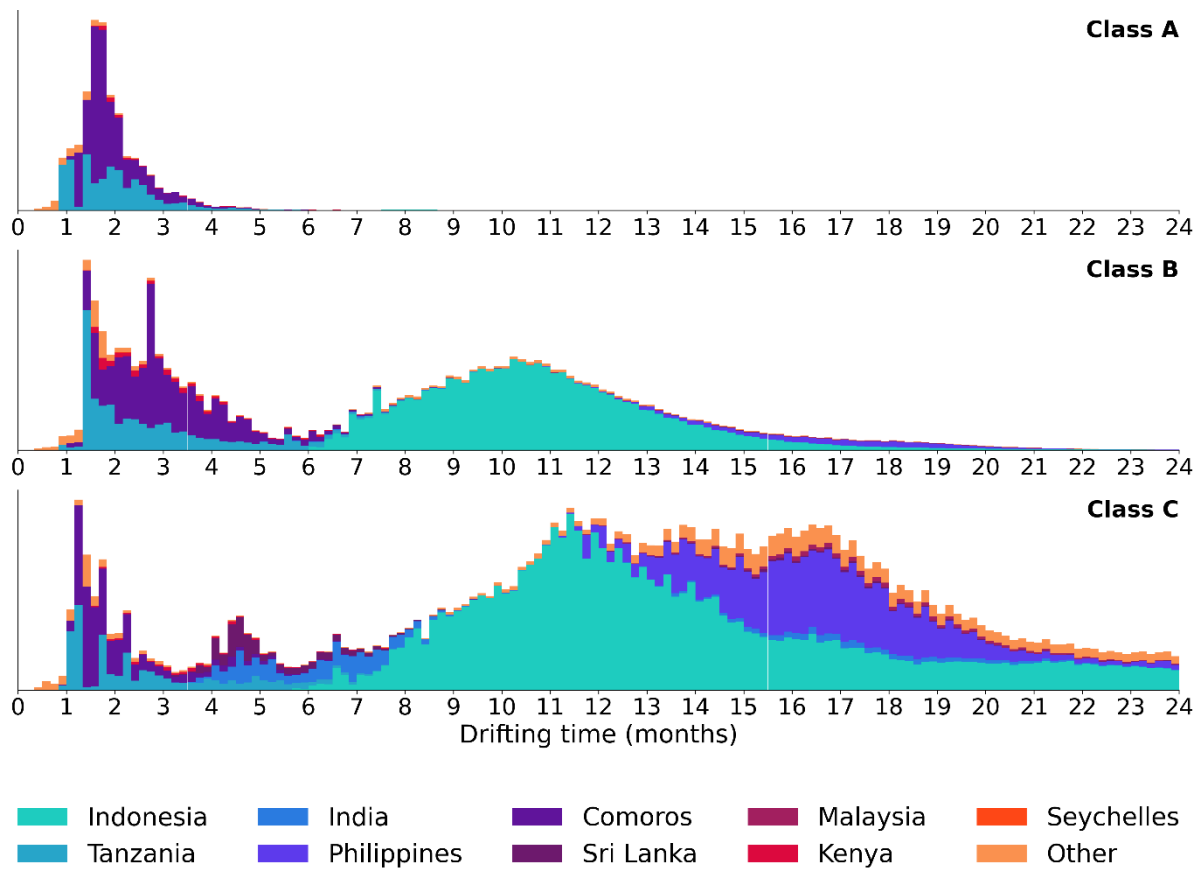


**Figure 8:** Drift time distribution of Class A, Class B, and Class C debris accumulating at Aldabra (y-axis normalised for comparison).

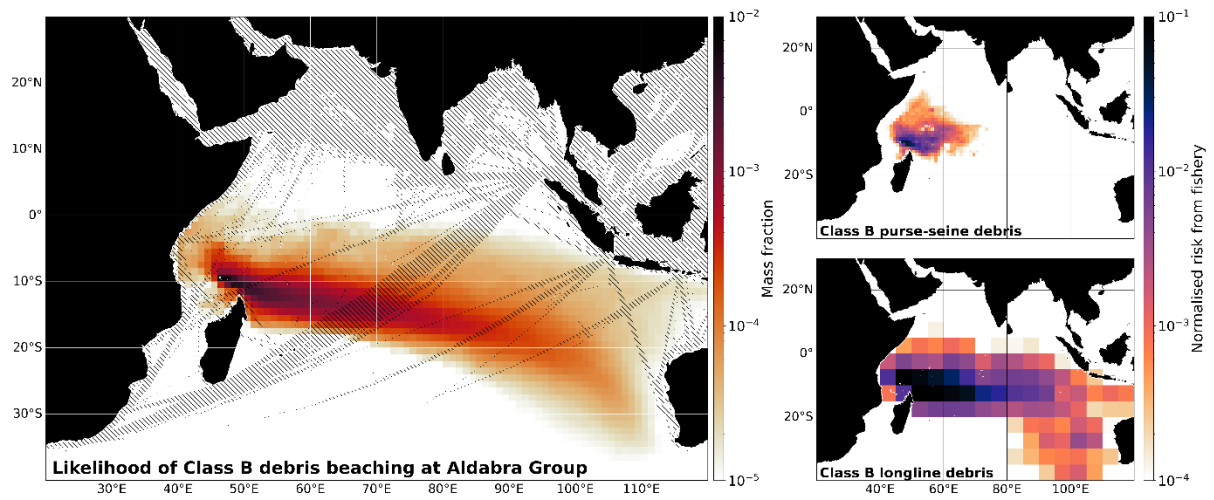


Figure 9: Risk maps for Class B debris beaching at the Aldabra Group (see Figure 5 in the main text).

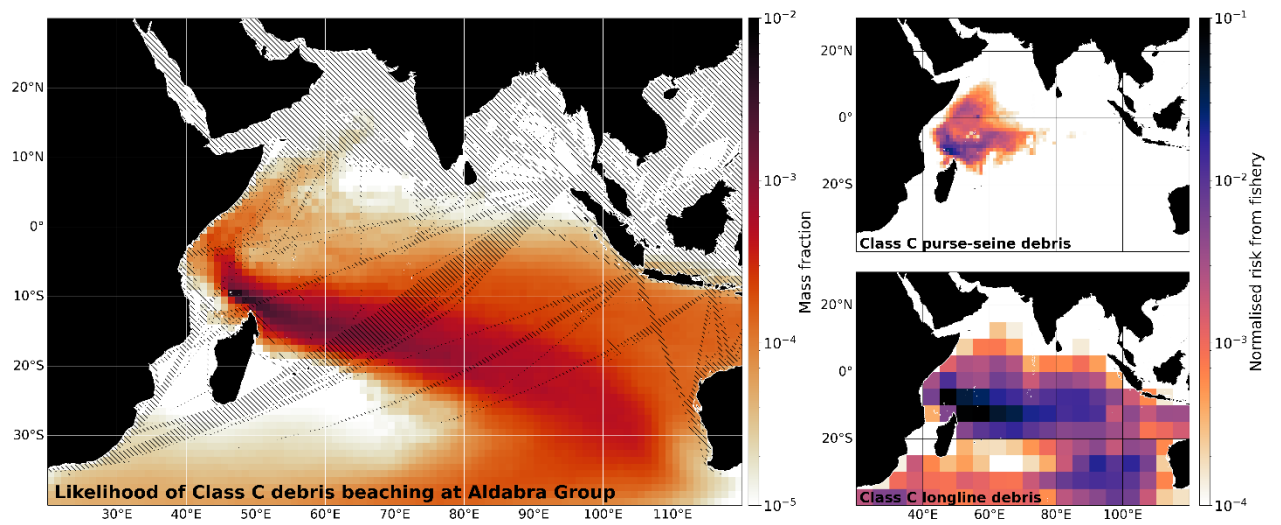


Figure 10: Risk maps for Class C debris beaching at the Aldabra Group (see Figure 5 in the main text).

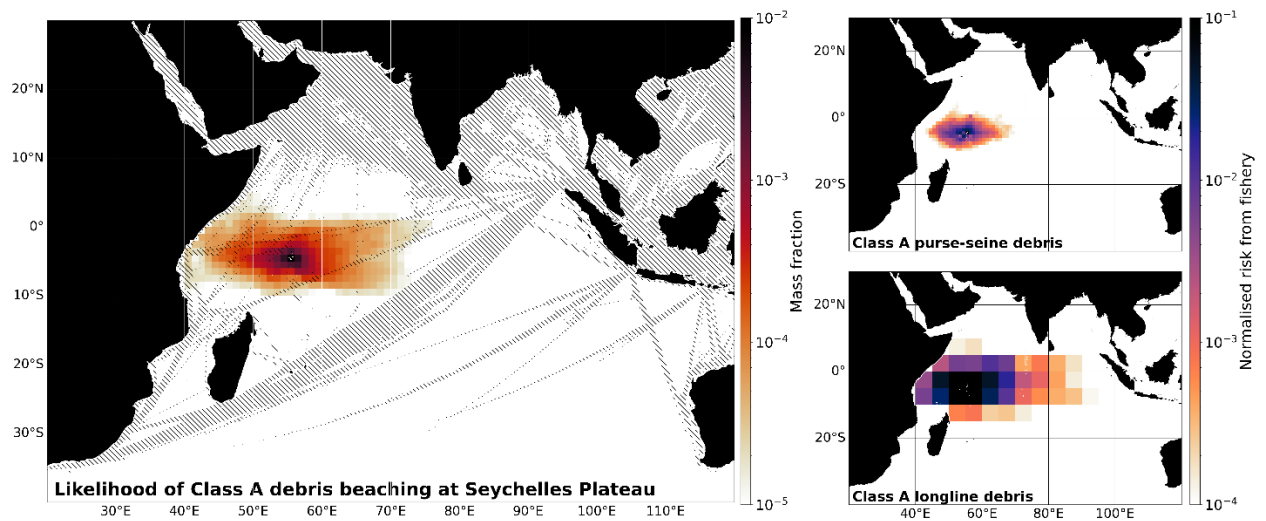


Figure 11: Risk maps for Class A debris beaching at the Seychelles Plateau (see Figure 5 in the main text).



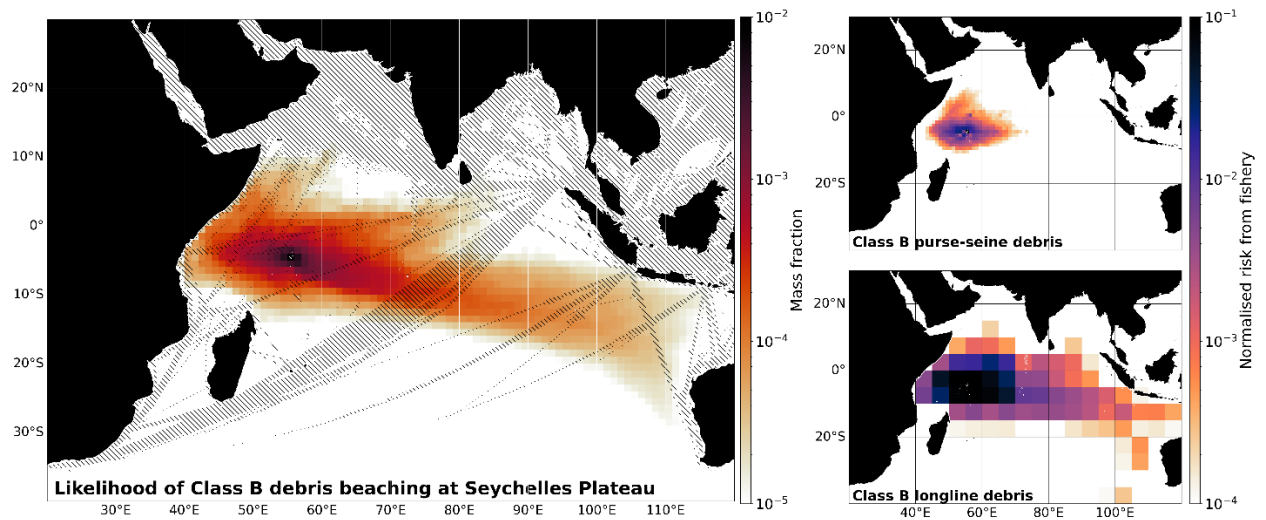


Figure 12: Risk maps for Class B debris beaching at the Seychelles Plateau (see Figure 5 in the main text).

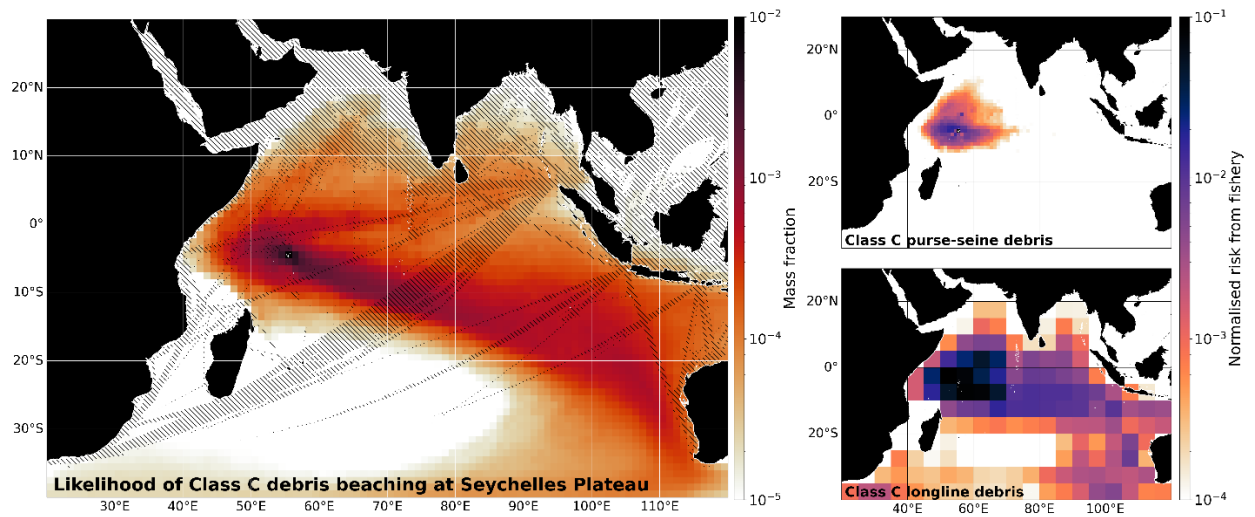


Figure 13: Risk maps for Class C debris beaching at the Seychelles Plateau (see Figure 5 in the main text).

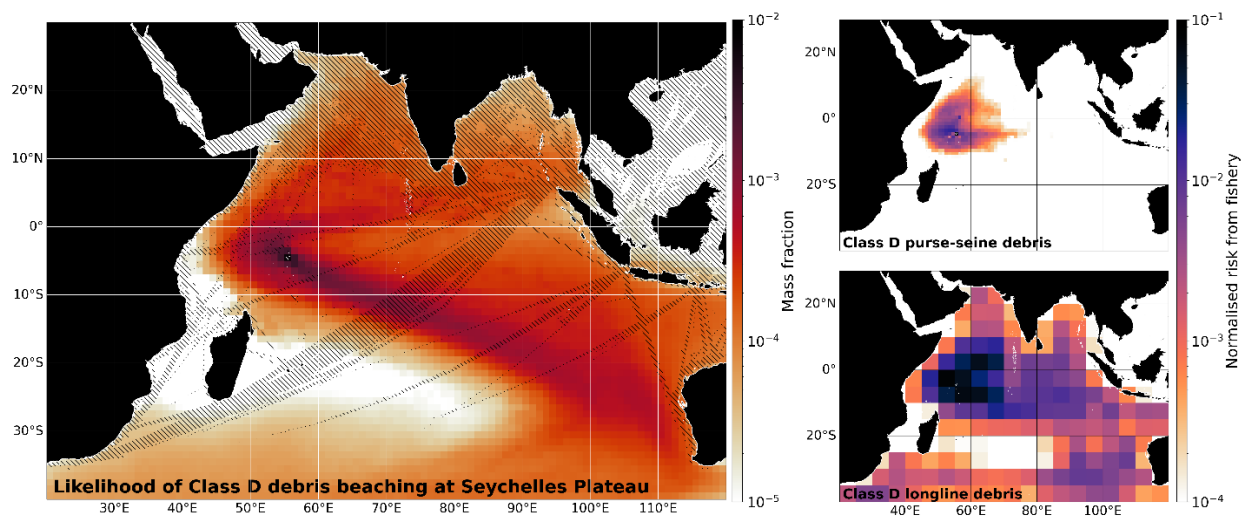
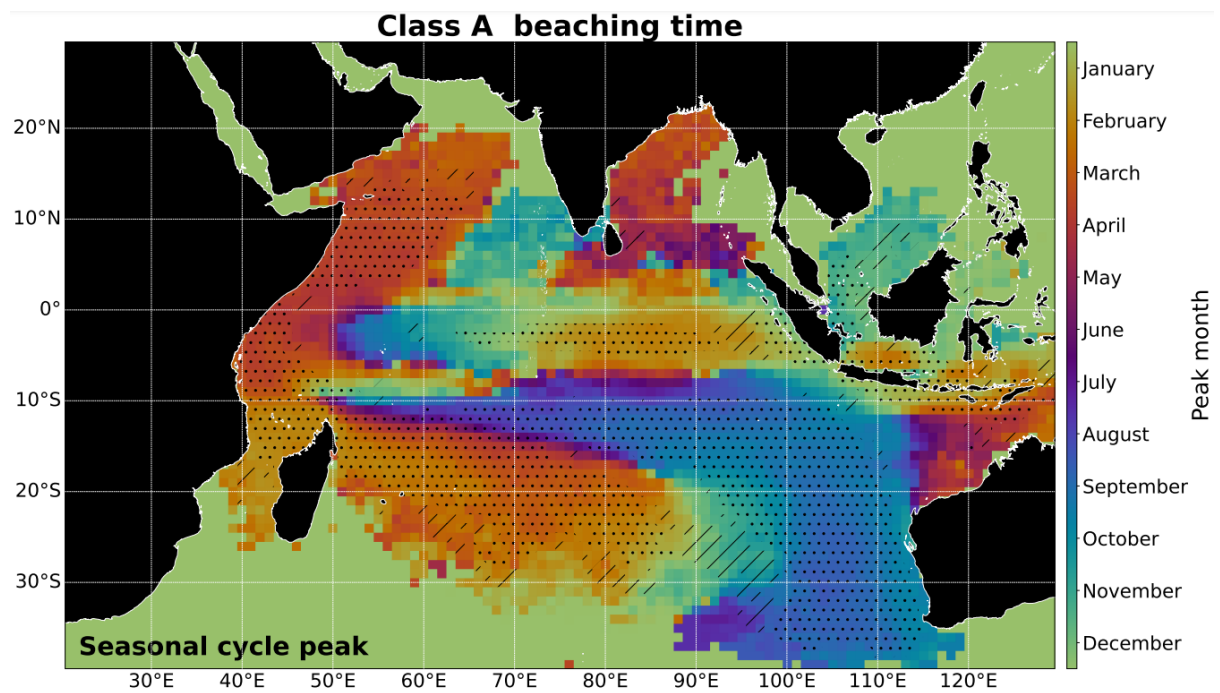
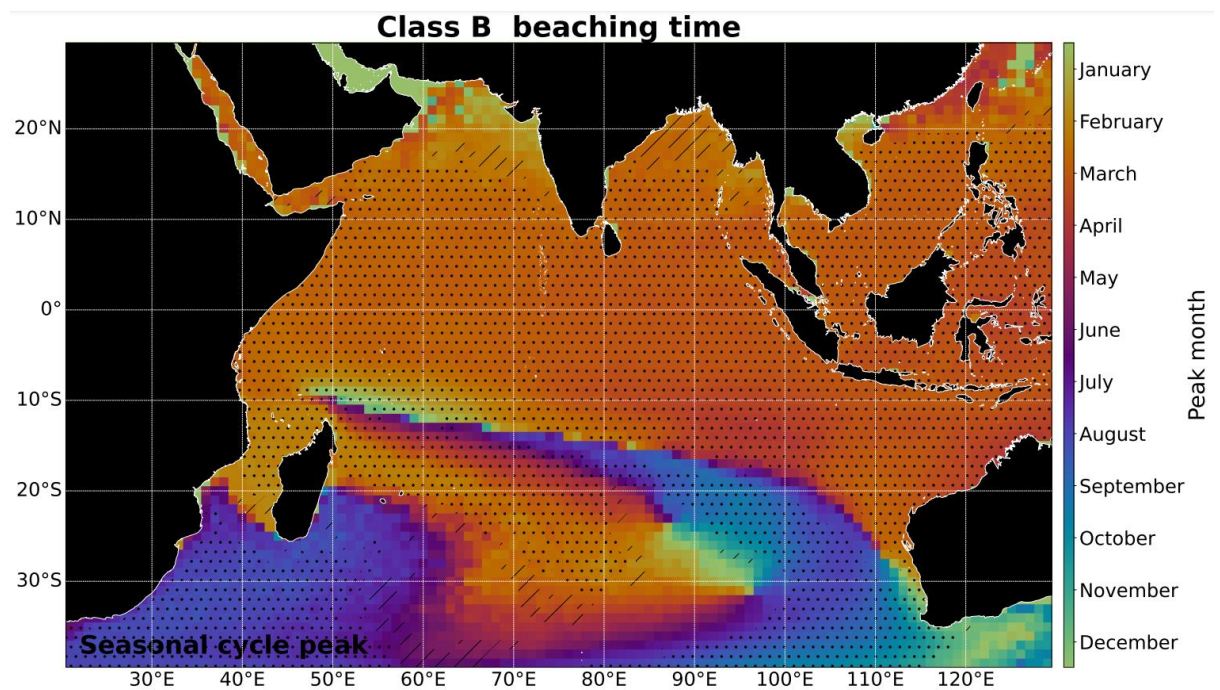


Figure 14: Risk maps for Class D debris beaching at the Seychelles Plateau (see Figure 5 in the main text).





*Figure 15: Phase of the seasonal cycle for Class A debris beaching at the Aldabra Group, i.e. when debris is most likely to beach at the Aldabra Group for a uniform seeding rate.*



*Figure 16: Phase of the seasonal cycle for Class B debris beaching at the Aldabra Group*

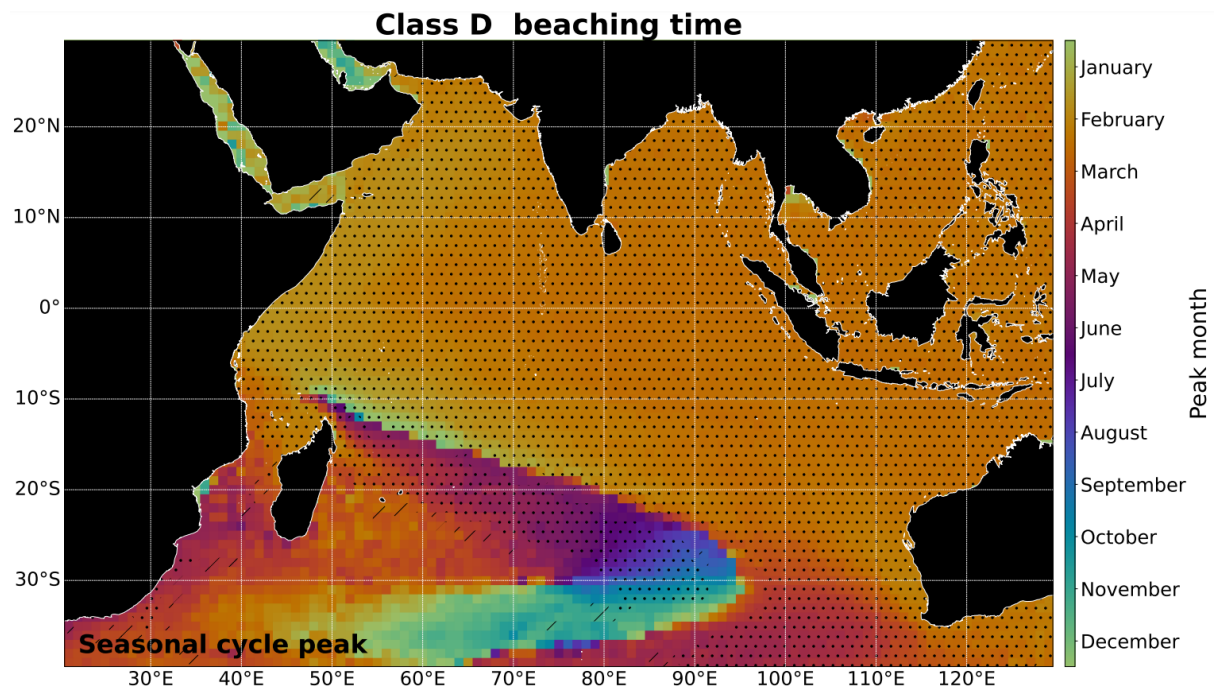


Figure 17: Phase of the seasonal cycle for Class D debris beaching at the Aldabra Group

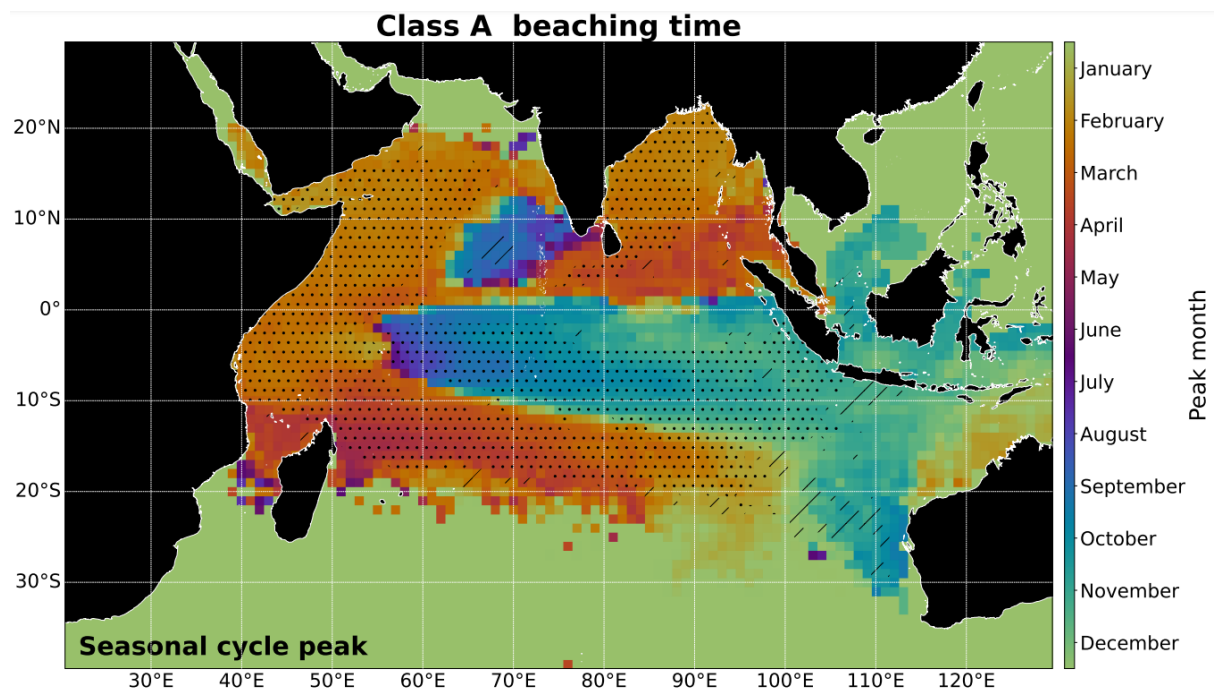
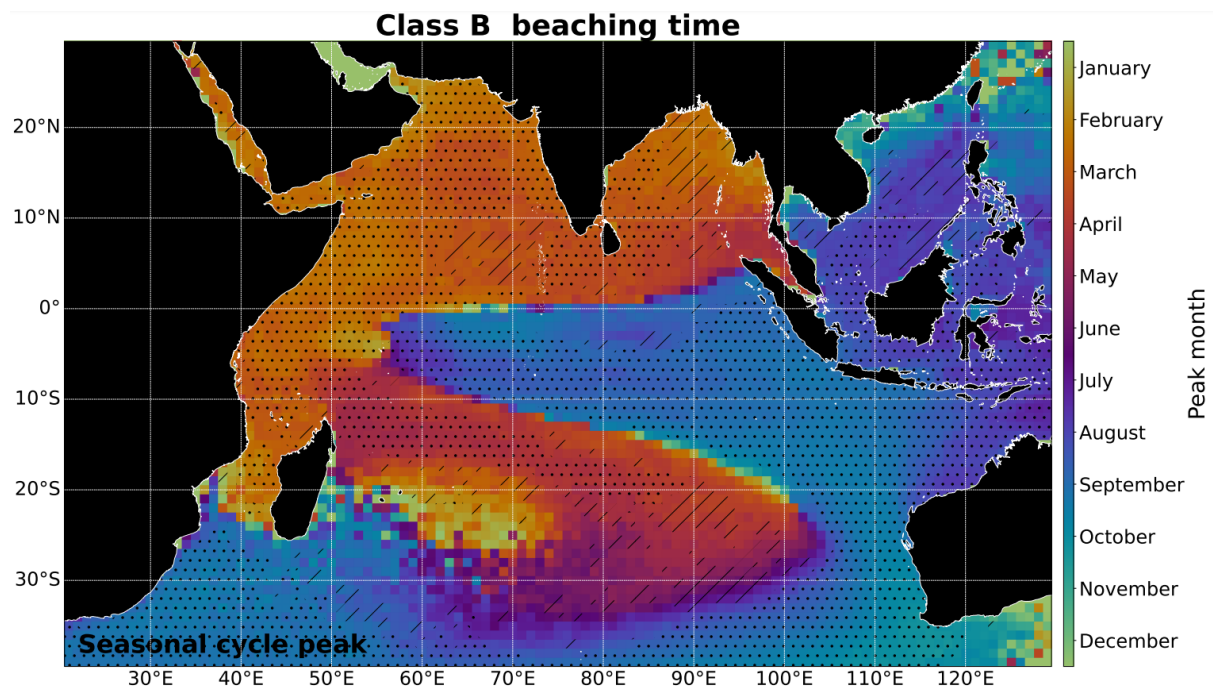
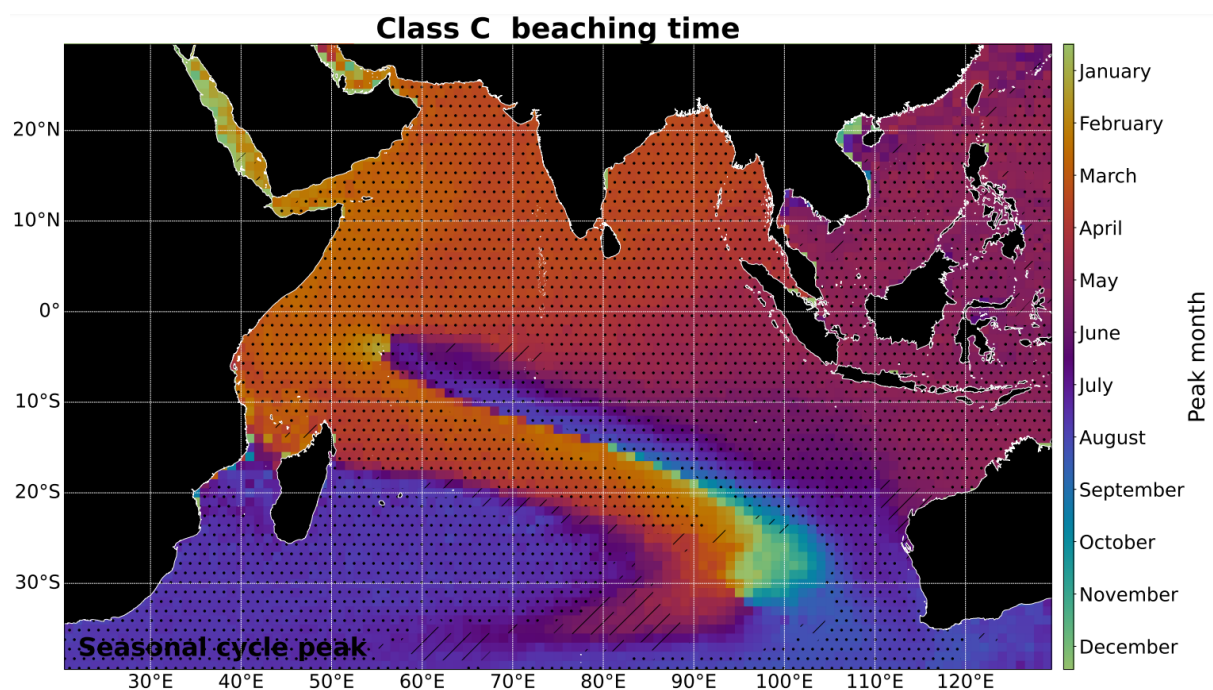


Figure 18: Phase of the seasonal cycle for Class A debris beaching at the Seychelles Plateau



*Figure 19: Phase of the seasonal cycle for Class B debris beaching at the Seychelles Plateau*



*Figure 20: Phase of the seasonal cycle for Class C debris beaching at the Seychelles Plateau. Note how the phase for Indonesia (May-June) contradicts the September-October 'peak' attributed to Indonesia in Figure 6(d) in the main text. This is because, as described in the main text, the September-October 'peak' is driven by a small number of beaching pulses and is not consistent. This spectral analysis suggests that the Class C pathway from Indonesia to the Seychelles Plateau most consistently terminates in May-June, not September-October.*



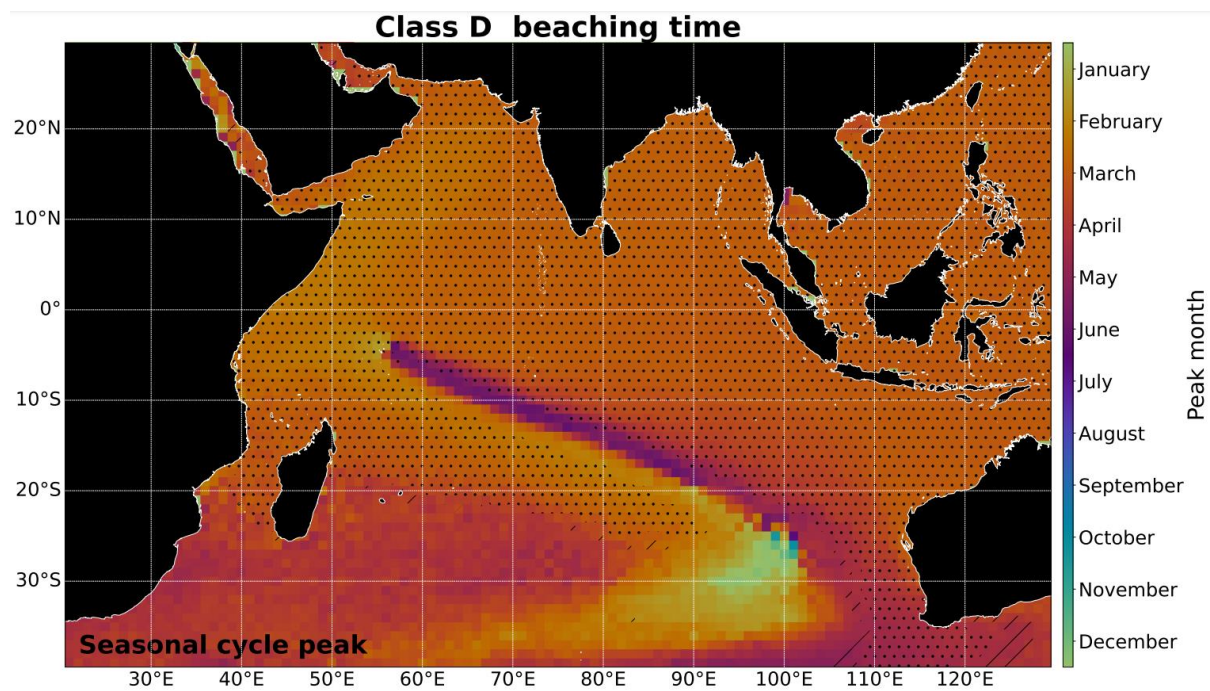


*Figure 21: Phase of the seasonal cycle for Class D debris beaching at the Seychelles Plateau*

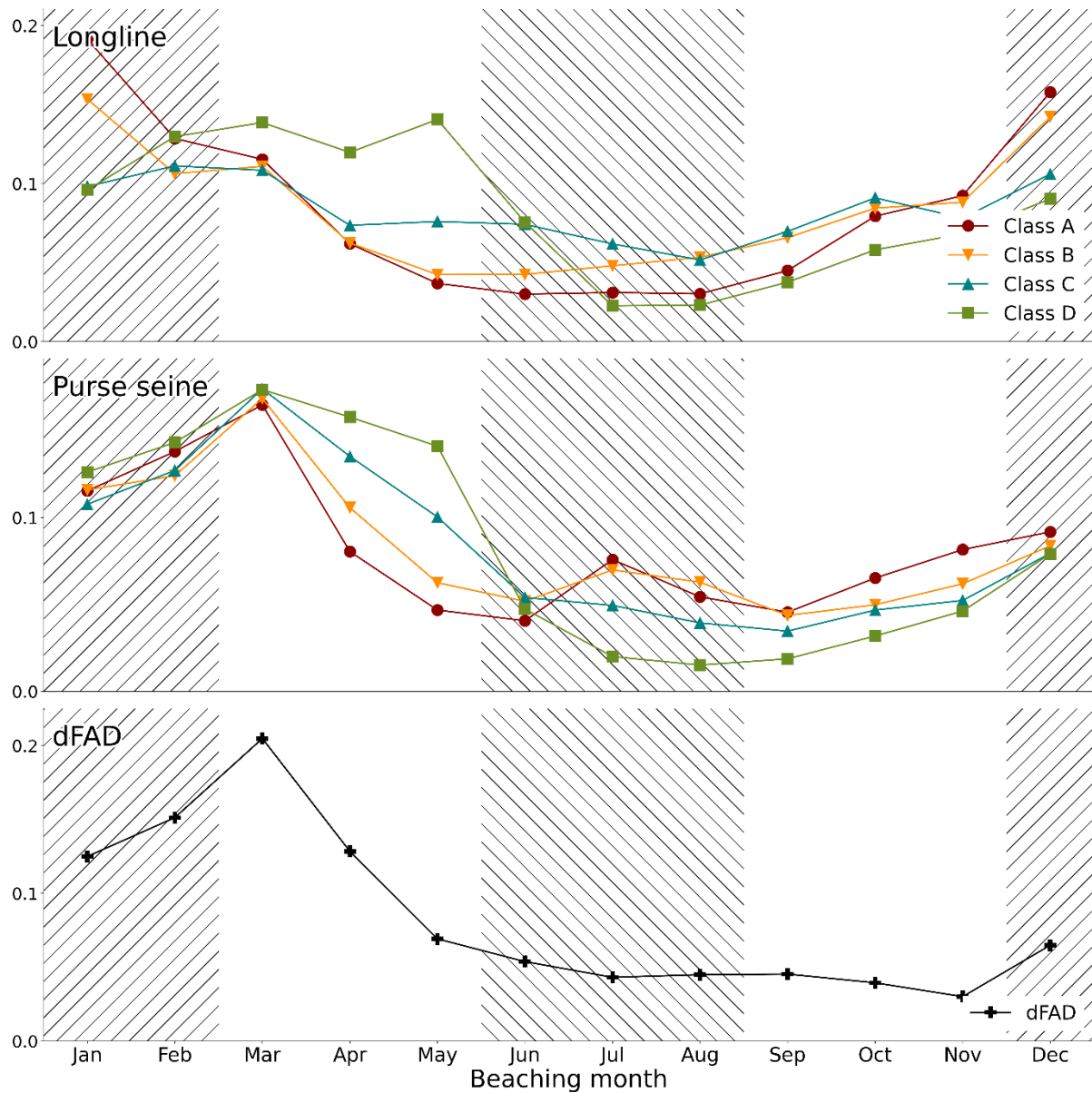


**Figure 22:** (a)-(b) Monthly beaching rate from 1995-2012 at the Seychelles Plateau for debris related to (a) Longlines and (b) Purse-seines, for Class A-D debris. (c) Predicted monthly beaching rate from 1995-2012 at the Seychelles Plateau of dFADs (2014-2019).

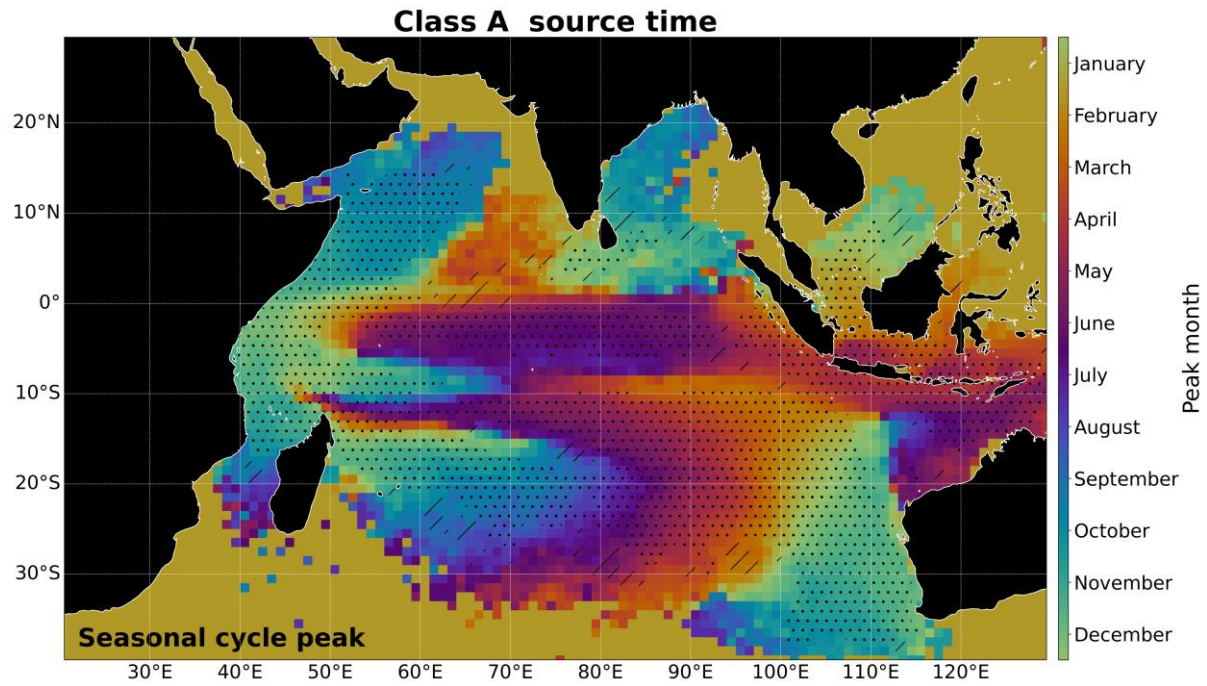


*Figure 23: Phase of the seasonal cycle of risk (source time) for Class A debris eventually beaching at the Aldabra Group, i.e. when in the year is debris entering the ocean most vulnerable to eventually beaching at the Aldabra Group. These are the months in which it is most important to avoid losing debris into the sea.*

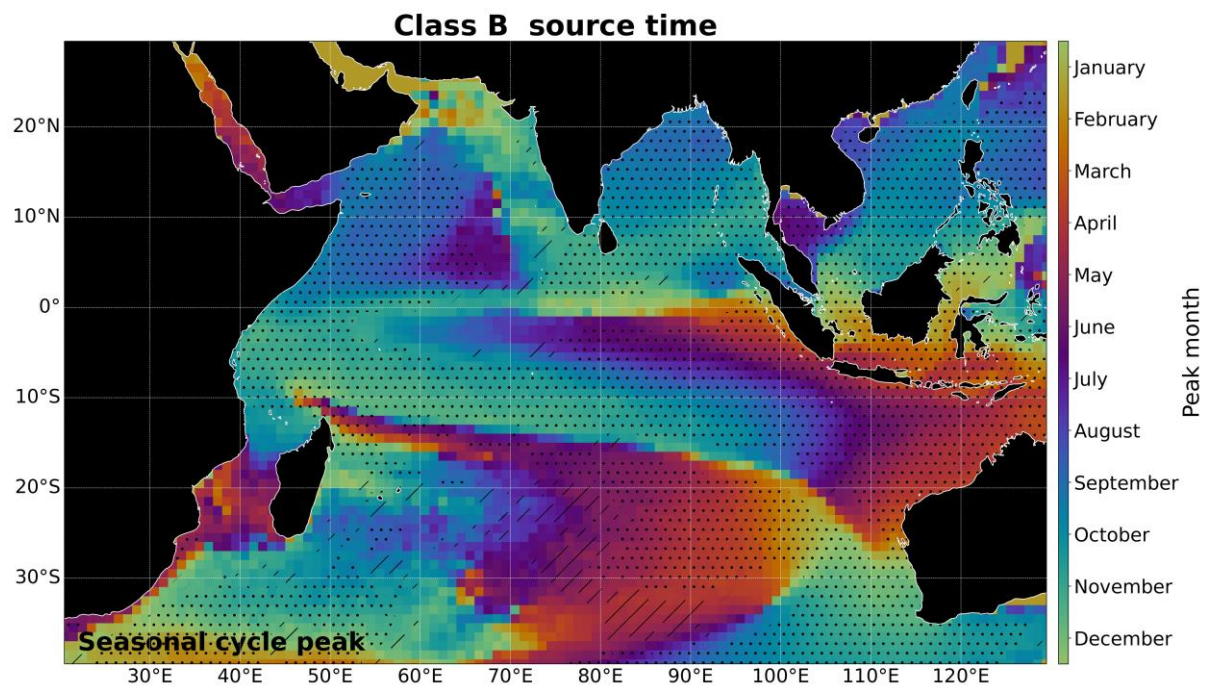


*Figure 24: Phase of the seasonal cycle of risk (source time) for Class B debris eventually beaching at the Aldabra Group.*



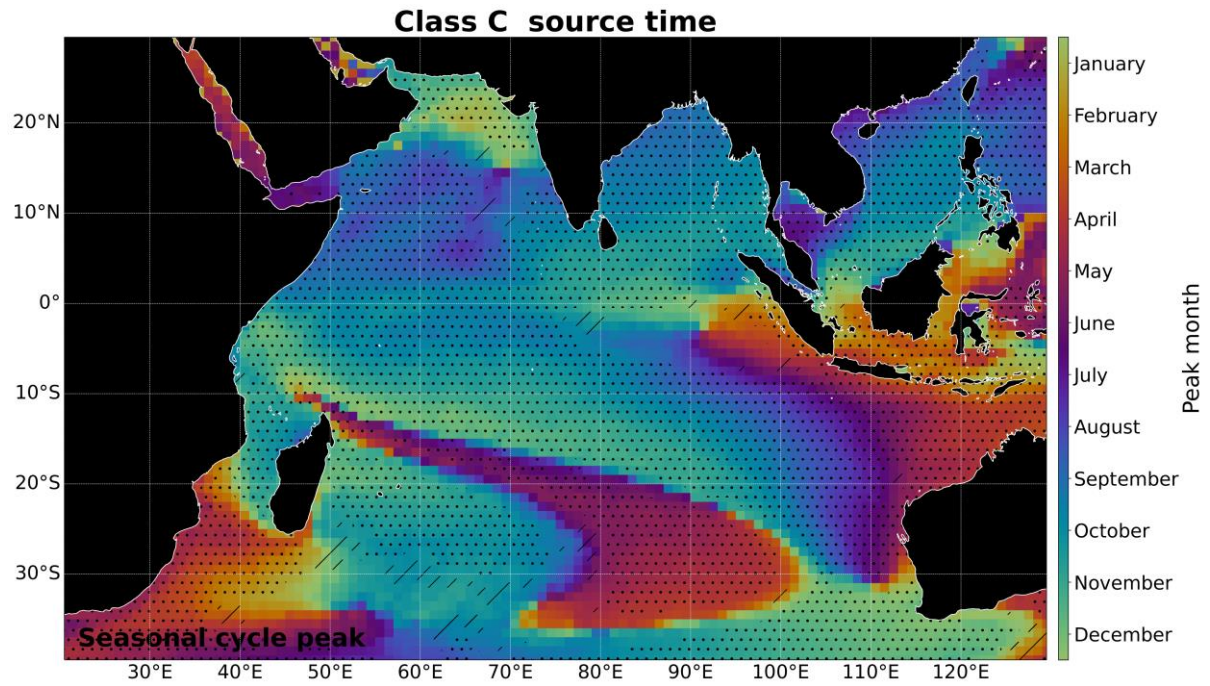


*Figure 25: Phase of the seasonal cycle of risk (source time) for Class C debris eventually beaching at the Aldabra Group.*

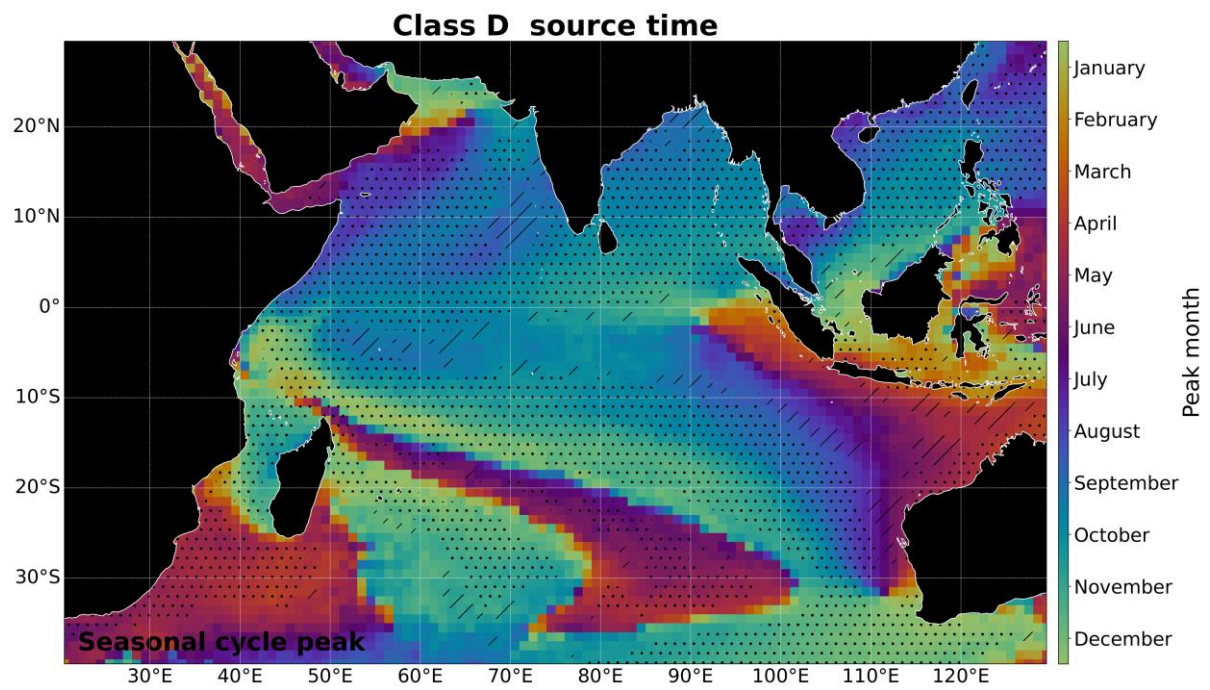


*Figure 26: Phase of the seasonal cycle of risk (source time) for Class D debris eventually beaching at the Aldabra Group.*

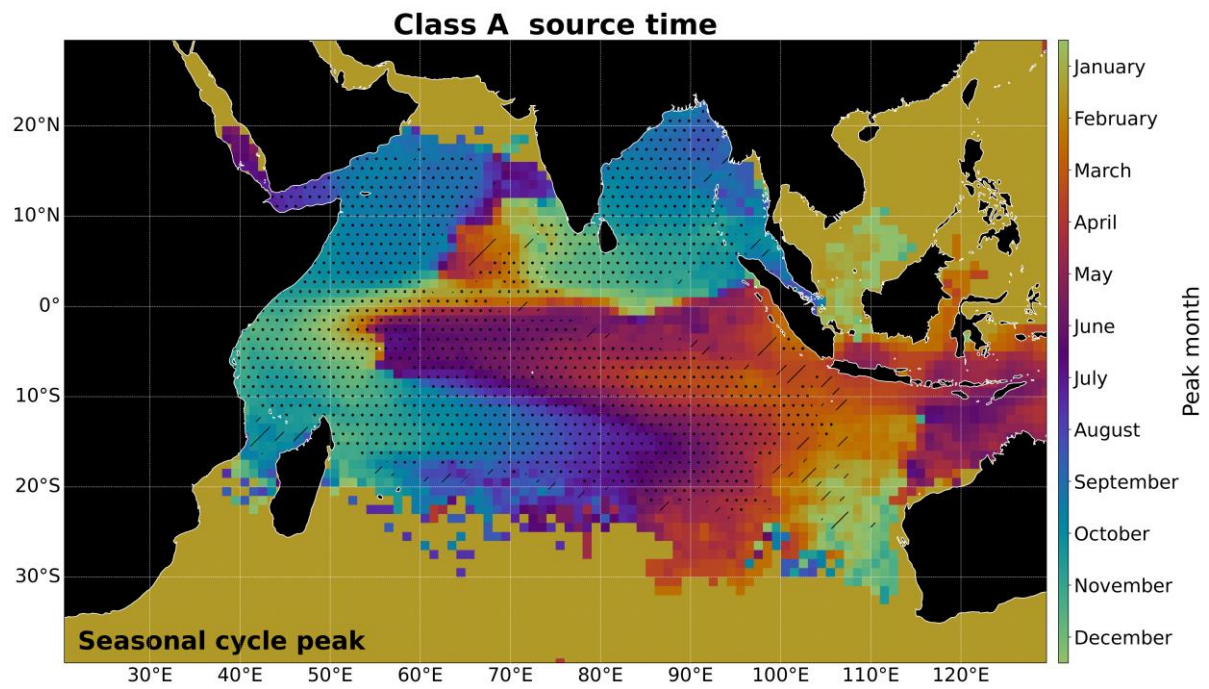


*Figure 27: Phase of the seasonal cycle of risk (source time) for Class A debris eventually beaching at the Seychelles Plateau.*

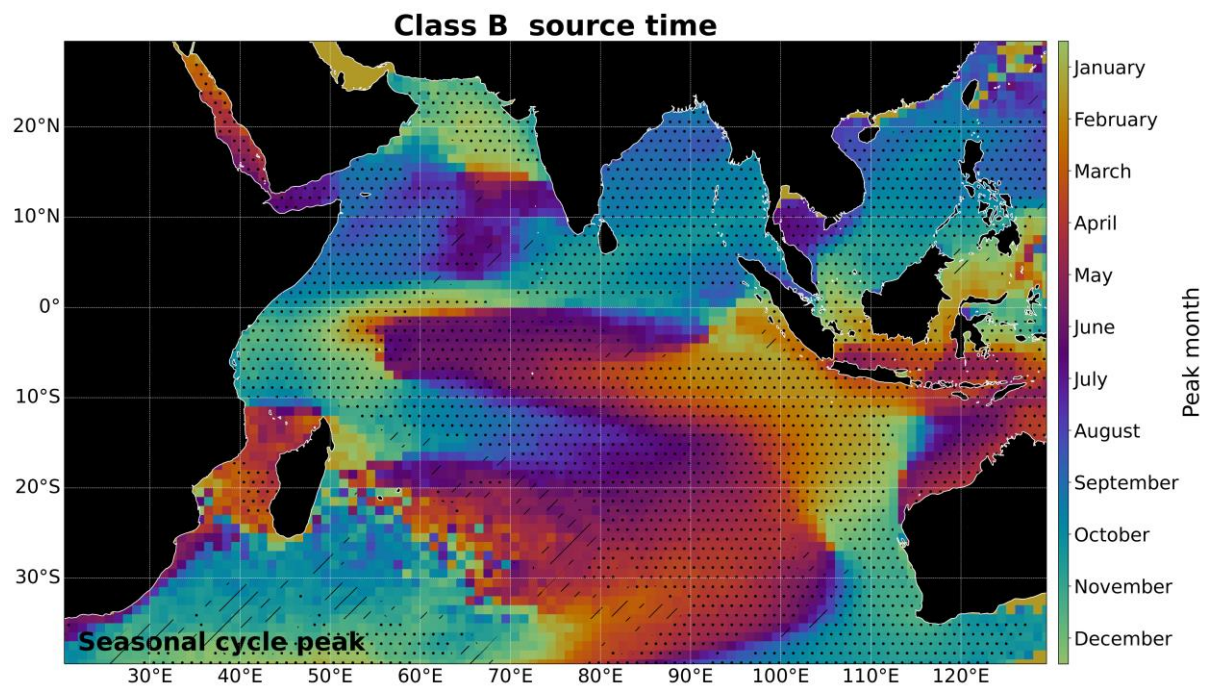


*Figure 28: Phase of the seasonal cycle of risk (source time) for Class B debris eventually beaching at the Seychelles Plateau.*



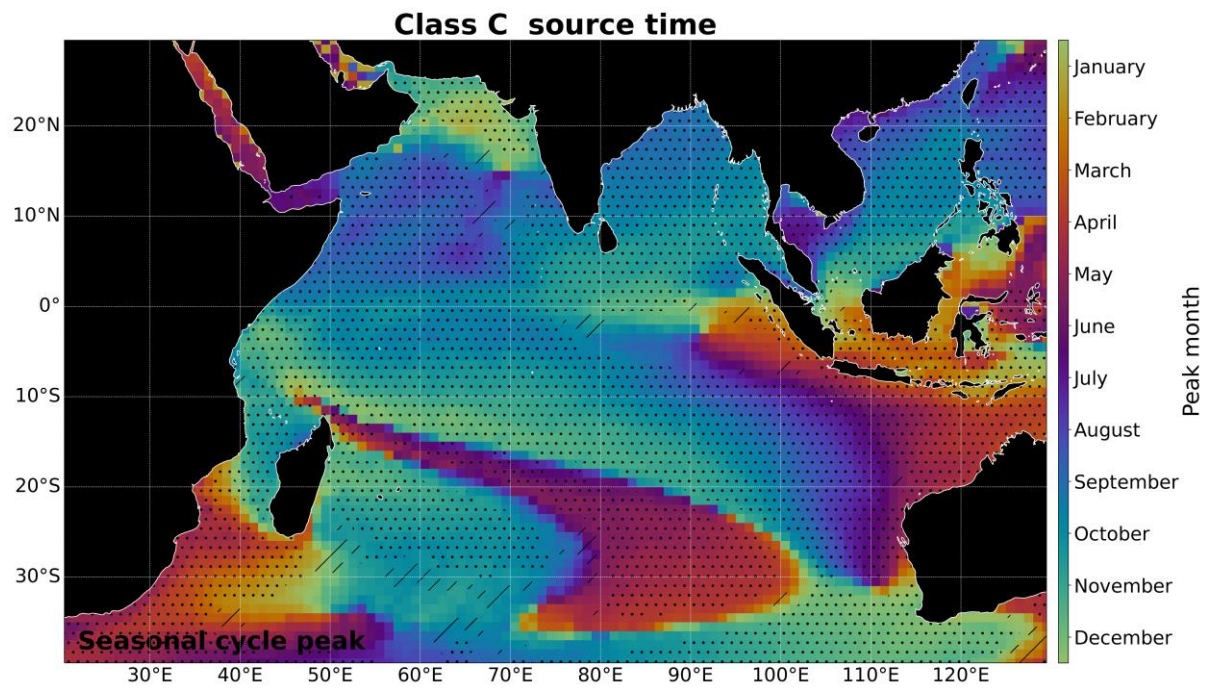


*Figure 29: Phase of the seasonal cycle of risk (source time) for Class C debris eventually beaching at the Seychelles Plateau.*

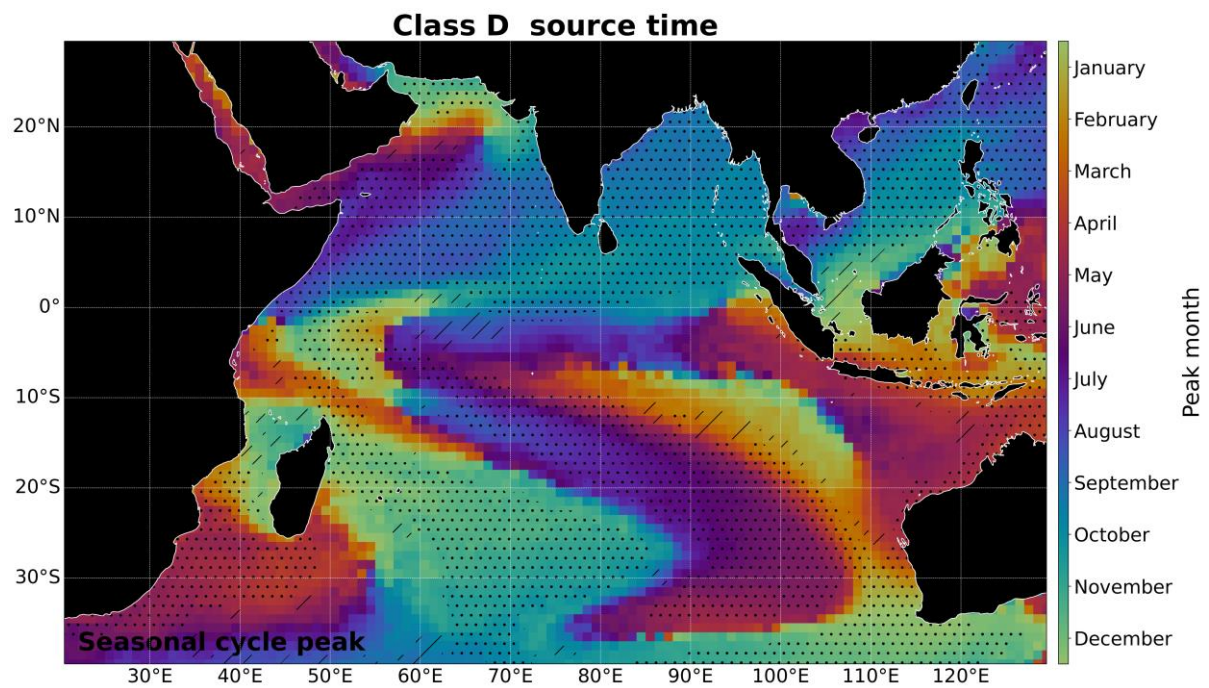


*Figure 30: Phase of the seasonal cycle of risk (source time) for Class D debris eventually beaching at the Seychelles Plateau.*

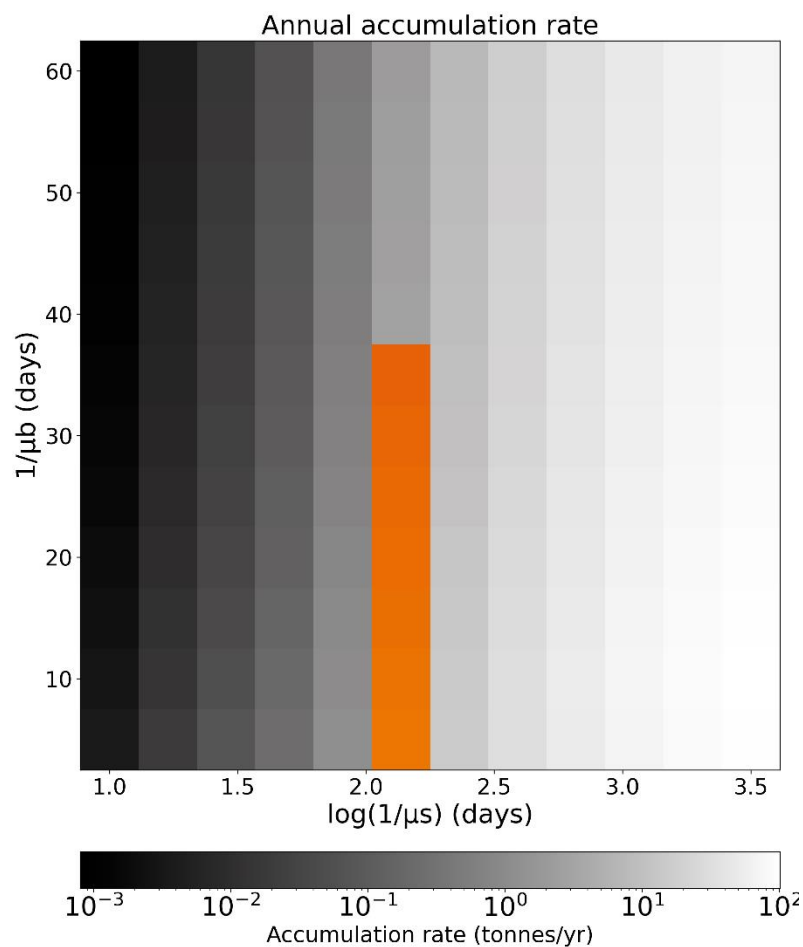


**Figure 31:** Mean annual beaching rate of debris at Aldabra for physical scenario **CS0**, as a function of the sinking and beaching rates. The range of accumulation rates consistent with observations at Aldabra (see main text 3.3.1) is highlighted in orange.

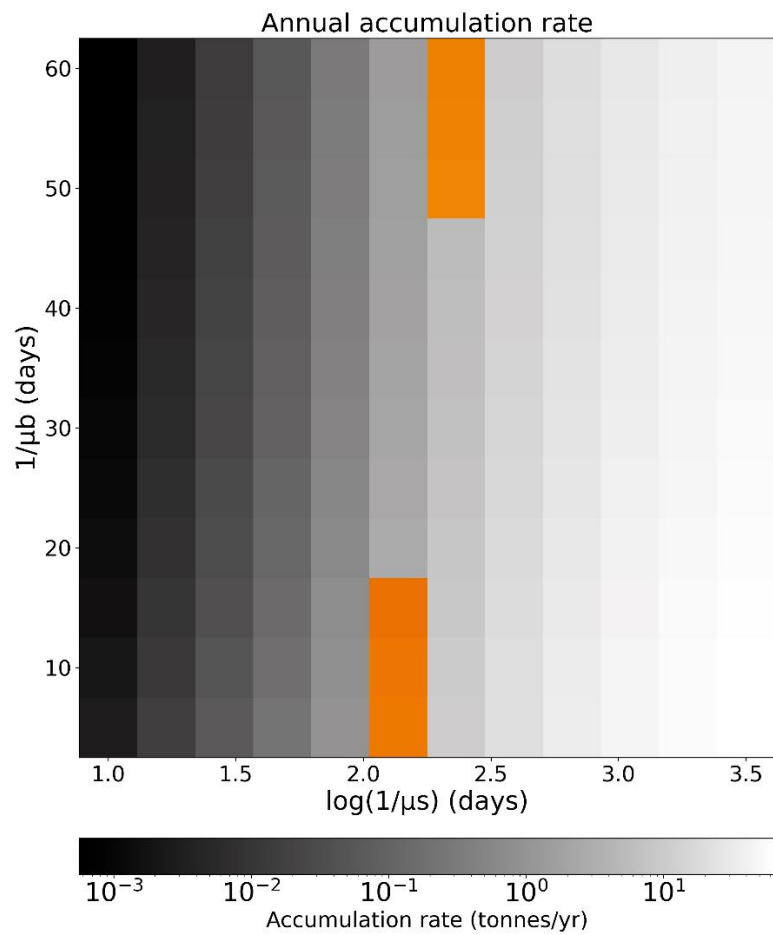


**Figure 32:** Mean annual beaching rate of debris at Aldabra for physical scenario **CS1**, as a function of the sinking and beaching rates. The range of accumulation rates consistent with observations at Aldabra (see main text 3.3.1) is highlighted in orange.

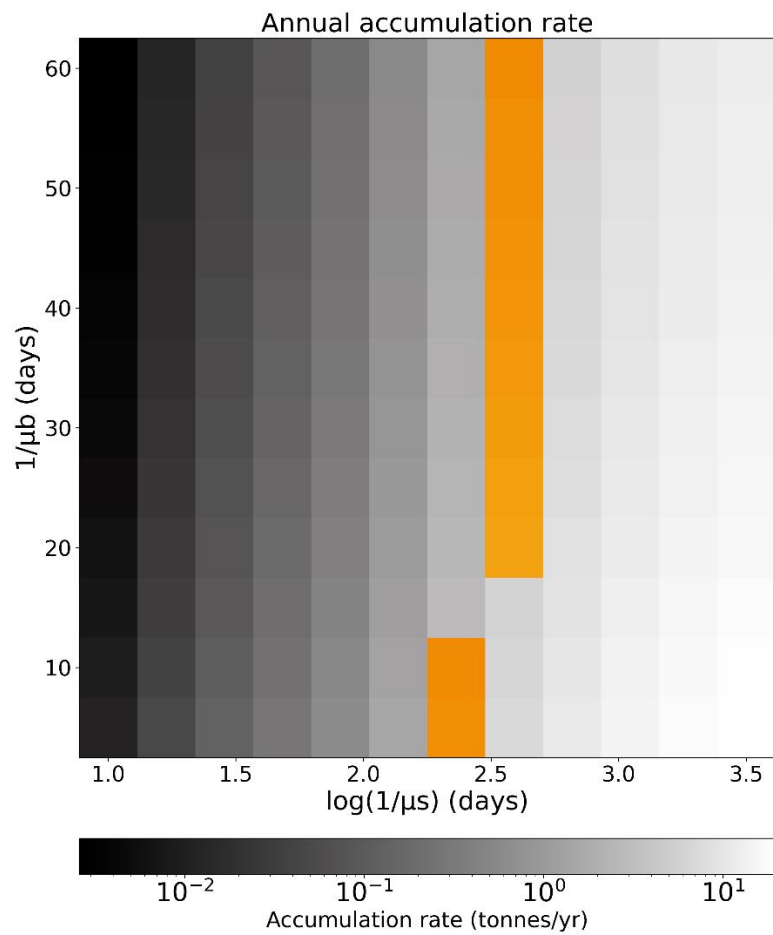


**Figure 33:** Mean annual beaching rate of debris at Aldabra for physical scenario **CS3**, as a function of the sinking and beaching rates. The range of accumulation rates consistent with observations at Aldabra (see main text 3.3.1) is highlighted in orange.

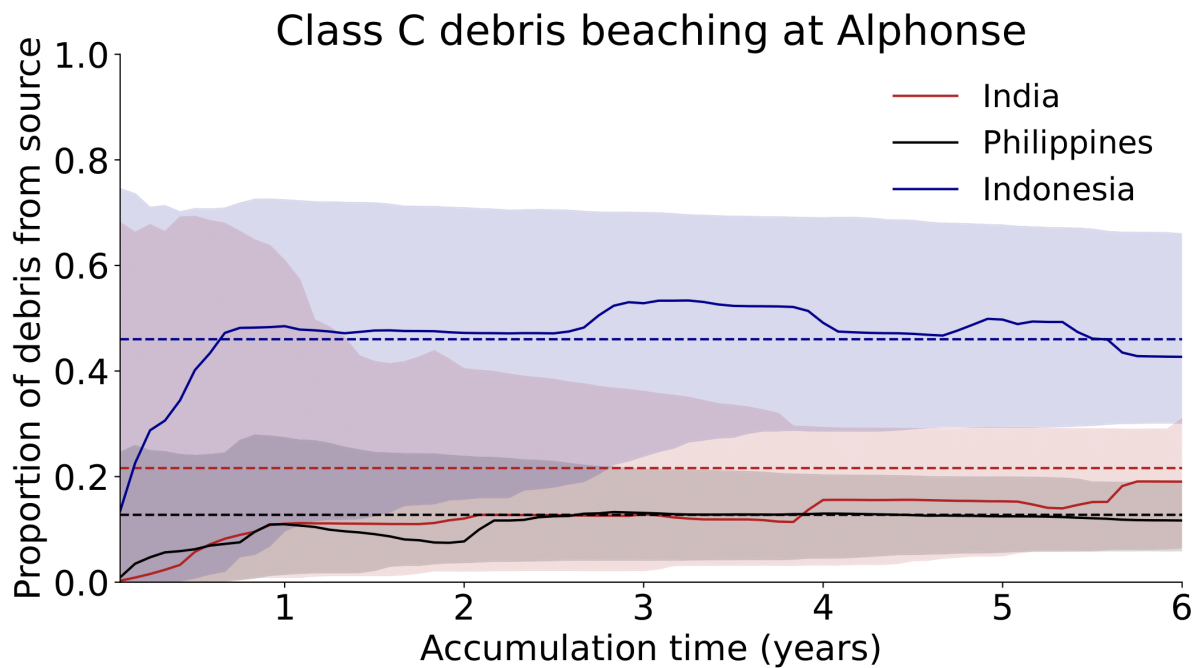


**Figure 34:** Proportion of debris from three major source countries of Class C debris at Alphonse, as a function of accumulation time. In this analysis, we compute the cumulative proportion of Class C debris beaching at Alphonse from India, Philippines, and Indonesia, across 168 6-year periods between 1993-2014 (e.g. Jan 1993 – Dec 1998, Feb 1993 – Jan 1999, ... , Jan 2009 – Dec 2014). The bold line shows the median proportion of debris across the 168 6-year periods, and the shaded region spans the 5<sup>th</sup>-95<sup>th</sup> percentile. The horizontal dashed line shows the time-mean proportion of debris across the 20 year period 1993-2014. The median estimates approach the ‘true’ time-mean value after about 6 months, but the range depending on the starting time of the accumulation period is very large. For instance, the 5<sup>th</sup>-95<sup>th</sup> percentile range for Class C debris from India and Indonesia only stop overlapping after around 4 years of accumulation, despite the time-mean flux of Class C debris from Indonesia being more than double that for India.

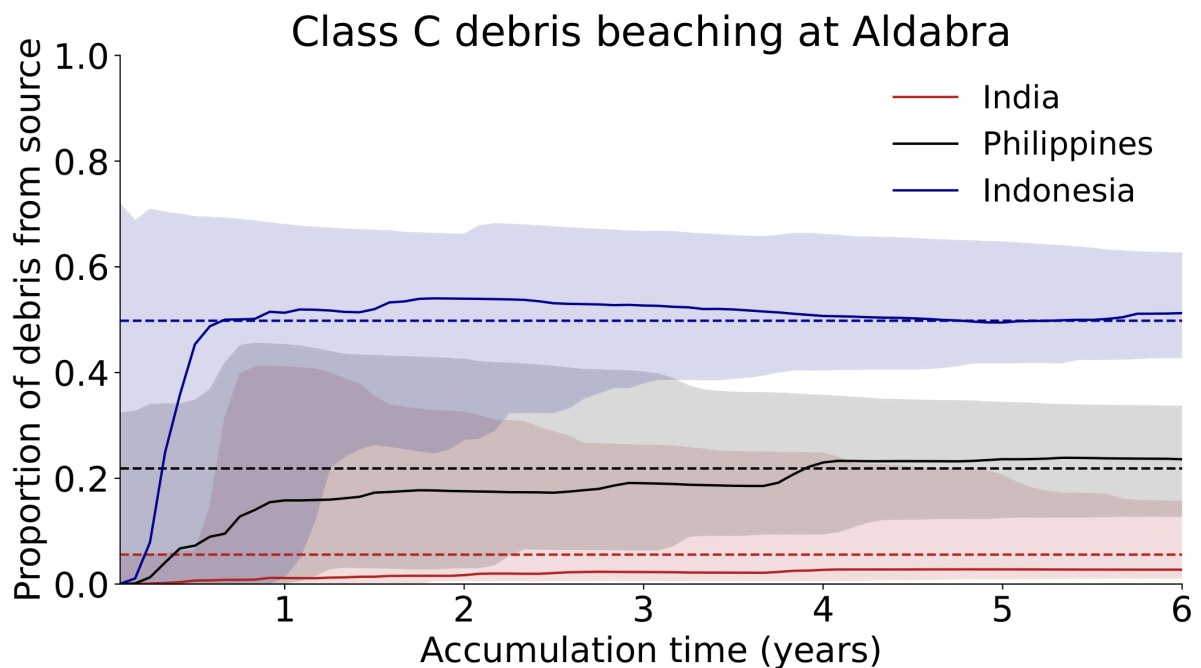


**Figure 35:** As in Figure 23, but for Class C debris beaching at Aldabra.

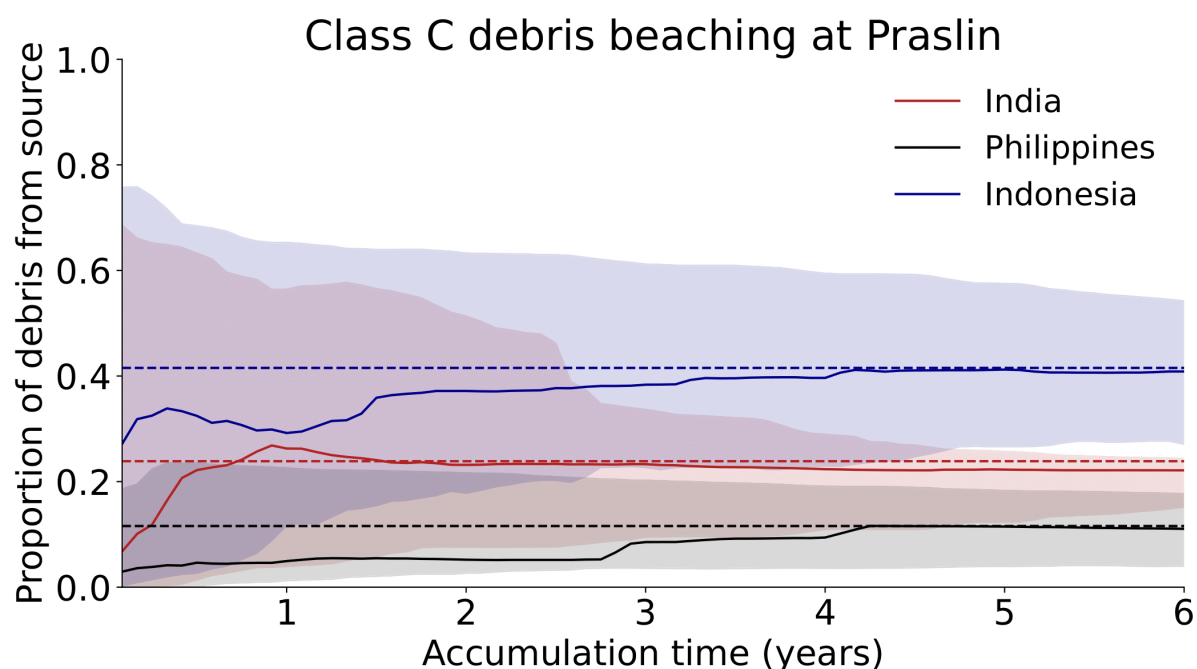


Figure 36: As in Figure 24, but for Class C debris beaching at Praslin.

## References

- Burt, A. J., Raguain, J., Sanchez, C., Brice, J., Fleischer-Dogley, F., Goldberg, R., Talma, S., Syposz, M., Mahony, J., Letori, J., Quanz, C., Ramkalawan, S., Francourt, C., Capricieuse, I., Antao, A., Belle, K., Zillhardt, T., Moumou, J., Roseline, M., ... Turnbull, L. A. (2020). The costs of removing the unsanctioned import of marine plastic litter to small island states. *Scientific Reports*, 10(1), 1–10. <https://doi.org/10.1038/s41598-020-71444-6>
- Chassignet, E. P., Xu, X., & Zavala-Romero, O. (2021). Tracking Marine Litter With a Global Ocean Model: Where Does It Go? Where Does It Come From? *Frontiers in Marine Science*, 8(April), 1–15. <https://doi.org/10.3389/fmars.2021.667591>
- Dunlop, S. W., Dunlop, B. J., & Brown, M. (2020). Plastic pollution in paradise: Daily accumulation rates of marine litter on Cousine Island, Seychelles. *Marine Pollution Bulletin*, 151(December 2019), 110803. <https://doi.org/10.1016/j.marpolbul.2019.110803>
- Geyer, R., Jambeck, J. R., & Law, K. L. (2017). Production, use, and fate of all plastics ever made. *Science Advances*, 3(7), 25–29. <https://doi.org/10.1126/sciadv.1700782>
- Imzilen, T., Lett, C., Chassot, E., & Kaplan, D. M. (2021). Spatial management can significantly reduce dFAD beachings in Indian and Atlantic Ocean tropical tuna purse seine fisheries. *Biological Conservation*, 254(December 2020), 108939. <https://doi.org/10.1016/j.biocon.2020.108939>
- Kaandorp, M. L. A., Dijkstra, H. A., & Van Sebille, E. (2020). Closing the Mediterranean Marine Floating Plastic Mass Budget: Inverse Modeling of Sources and Sinks. *Environmental Science and Technology*, 54(19), 11980–11989. <https://doi.org/10.1021/acs.est.0c01984>
- Lebreton, L., & Andrady, A. (2019). Future scenarios of global plastic waste generation and disposal. *Palgrave Communications*, 5(1), 1–11. <https://doi.org/10.1057/s41599-018-0212-7>
- Lumpkin, R., & Centurioni, L. (2019). *Global Drifter Program quality-controlled 6-hour interpolated data from ocean surface drifting buoys*. <https://doi.org/10.25921/7ntx-z961>
- Lumpkin, R., Maximenko, N., & Pazos, M. (2012). Evaluating where and why drifters die. *Journal of Atmospheric and Oceanic Technology*, 29(2), 300–308. <https://doi.org/10.1175/JTECH-D-11-00100.1>
- Meijer, L. J. J., van Emmerik, T., van der Ent, R., Schmidt, C., & Lebreton, L. (2021). More than 1000 rivers account for 80% of global riverine plastic emissions into the ocean. *Science Advances*,

7(18), 1–14. <https://doi.org/10.1126/sciadv.aaz5803>

Schulzweida, U. (2021). *CDO User Guide (Version 2.0.0)*. Zenodo.  
<https://doi.org/http://doi.org/10.5281/zenodo.5614769>

van der Mheen, M., van Sebille, E., & Pattiaratchi, C. (2020). Beaching patterns of plastic debris along the Indian Ocean rim. *Ocean Science Discussions*, 1–31. <https://doi.org/10.5194/os-2020-50>

Wessel, P., & Smith, W. H. F. (1996). A global, self-consistent, hierarchical, high-resolution shoreline database. *Journal of Geophysical Research B: Solid Earth*, 101(4), 8741–8743.  
<https://doi.org/10.1029/96jb00104>